Article

A substrate-specific mTORC1 pathway underlies Birt–Hogg–Dubé syndrome

https://doi.org/10.1038/s41586-020-2444-0

Received: 3 December 2019

Accepted: 27 April 2020

Published online: 1 July 2020

Check for updates

Gennaro Napolitano[1,2,10], Chiara Di Malta[1,10], Alessandra Esposito[1], Mariana E. G. de Araujo[3], Salvatore Pece[4,5], Giovanni Bertalot[4], Maria Matarese[1], Valerio Benedetti[1], Angela Zampelli[1], Taras Stasyk[3], Diletta Siciliano[1], Alessandro Venuta[1], Marcella Cesana[1], Claudia Vilardo[1], Edoardo Nusco[1], Jlenia Monfregola[1], Alessia Calcagni[6,7], Pier Paolo Di Fiore[4,5], Lukas A. Huber[3,8] & Andrea Ballabio[1,2,6,7,9] ✉

The mechanistic target of rapamycin complex 1 (mTORC1) is a key metabolic hub that controls the cellular response to environmental cues by exerting its kinase activity on multiple substrates[1–3]. However, whether mTORC1 responds to diverse stimuli by differentially phosphorylating specific substrates is poorly understood. Here we show that transcription factor EB (TFEB), a master regulator of lysosomal biogenesis and autophagy[4,5], is phosphorylated by mTORC1 via a substrate-specific mechanism that is mediated by Rag GTPases. Owing to this mechanism, the phosphorylation of TFEB—unlike other substrates of mTORC1, such as S6K and 4E-BP1— is strictly dependent on the amino-acid-mediated activation of RagC and RagD GTPases, but is insensitive to RHEB activity induced by growth factors. This mechanism has a crucial role in Birt–Hogg–Dubé syndrome, a disorder that is caused by mutations in the RagC and RagD activator folliculin (*FLCN*) and is characterized by benign skin tumours, lung and kidney cysts and renal cell carcinoma[6,7]. We found that constitutive activation of TFEB is the main driver of the kidney abnormalities and mTORC1 hyperactivity in a mouse model of Birt–Hogg–Dubé syndrome. Accordingly, depletion of TFEB in kidneys of these mice fully rescued the disease phenotype and associated lethality, and normalized mTORC1 activity. Our findings identify a mechanism that enables differential phosphorylation of mTORC1 substrates, the dysregulation of which leads to kidney cysts and cancer.

Activation of mTORC1 occurs at the lysosomal membrane and is known to be mediated by the small GTPase Ras homologue enriched in brain (RHEB), the activity of which is induced by growth factors and inhibited by the tuberous sclerosis complex (TSC)[8–11]. mTORC1 is recruited to the lysosomal membrane when Rag GTPase heterodimers (RagA or RagB (RagA/B) in complex with RagC or RagD (RagC/D)) are in the active configuration (that is, GTP-bound RagA/B and GDP-bound RagC/D)[12–14]. Rag activation is mediated by the nutrient-activated GTPase-activating proteins GATOR1 and FLCN, which modify the nucleotide state of RagA/B and RagC/D, respectively[15–18].

TFEB is a transcriptional controller of cell metabolism[4,5] and its activity is negatively regulated by mTORC1-mediated phosphorylation, which promotes the cytoplasmic localization and inhibits the nuclear translocation of TFEB[19–24]. It has previously been reported that mTORC1 and TFEB are part of a feedback loop in which mTORC1 negatively regulates TFEB, whereas TFEB—in turn—is able to positively regulate mTORC1 activity through transcriptional induction of RagC/D[25]. Here we describe an 'unconventional' mTORC1 substrate-recruitment mechanism that makes TFEB phosphorylation highly sensitive to amino acid availability but insensitive to growth factors, thus allowing a selective downstream response of mTORC1 to specific nutritional inputs. Dysfunction of this mechanism is a crucial determinant of Birt–Hogg–Dubé (BHD) syndrome, a disease caused by loss-of-function mutations of the mTORC1 regulator *FLCN*.

TFEB phosphorylation does not require RHEB

We investigated whether the phosphorylation of TFEB behaves differently from other substrates of mTORC1. Although both amino acid and serum deprivation inhibited phosphorylation of the mTORC1 substrates S6K and 4E-BP1, only amino acid deprivation was able to suppress TFEB phosphorylation (Fig. 1a, Extended Data Fig. 1a, b, d, f). Consistently, TFEB subcellular localization and activity were affected only by amino acid deprivation, whereas serum starvation had no effect (Fig. 1b, Extended Data Fig. 1c, e, g). In line with these observations, silencing *RHEB* and its homologue *RHEBL1* using short interfering (si) RNA did not affect the phosphorylation, subcellular localization or activity of TFEB, but severely impaired the phosphorylation of S6K

[1]Telethon Institute of Genetics and Medicine (TIGEM), Naples, Italy. [2]Medical Genetics Unit, Department of Medical and Translational Science, Federico II University, Naples, Italy. [3]Institute of Cell Biology, Biocenter, Medical University of Innsbruck, Innsbruck, Austria. [4]IEO, European Institute of Oncology IRCCS, Milan, Italy. [5]Department of Oncology and Hemato-Oncology, University of Milan, Milan, Italy. [6]Department of Molecular and Human Genetics, Baylor College of Medicine, Houston, TX, USA. [7]Jan and Dan Duncan Neurological Research Institute, Texas Children's Hospital, Houston, TX, USA. [8]Austrian Drug Screening Institute (ADSI), Innsbruck, Austria. [9]SSM School for Advanced Studies, Federico II University, Naples, Italy. [10]These authors contributed equally: Gennaro Napolitano, Chiara Di Malta. ✉e-mail: ballabio@tigem.it

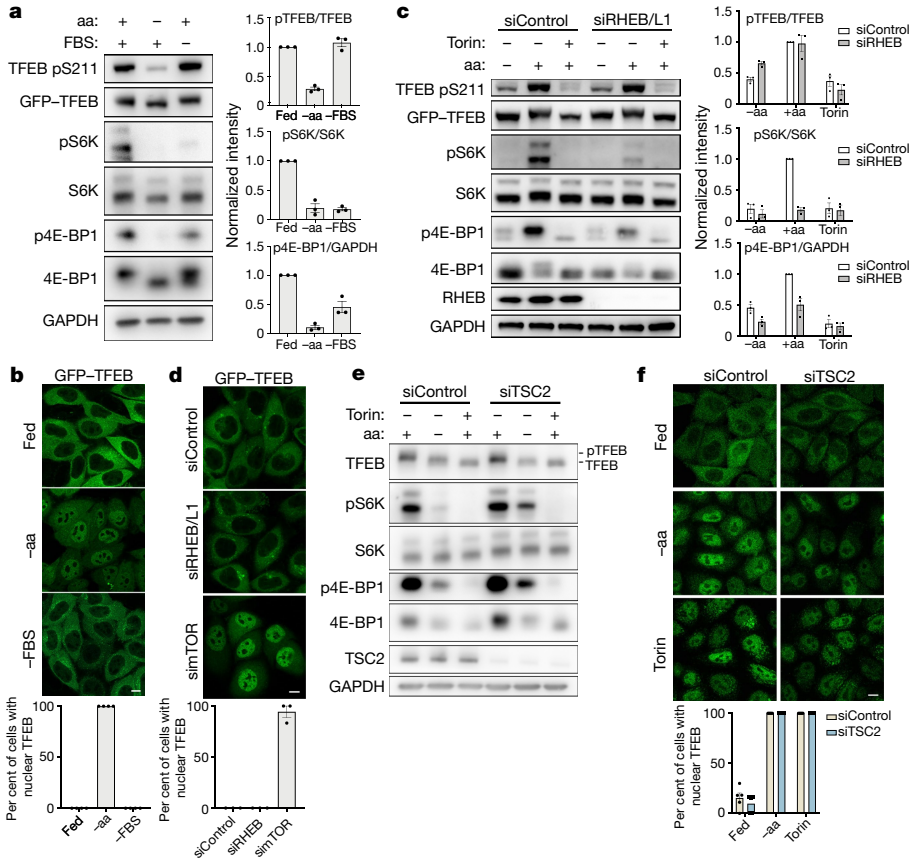

Fig. 1 | TFEB phosphorylation is insensitive to the RHEB–TSC axis. **a**, Representative immunoblotting and quantification (mean ± s.e.m.; $n = 3$ experiments) of HeLa cells that stably express GFP–TFEB starved of either amino acids (aa) or serum (FBS) for 2 h. Plots on the right show phosphorylated (p)TFEB/TFEB (top), pS6K/S6K (middle) and p4E-BP1/GAPDH (bottom) ratios. Fed, cells provided with both amino acids and serum. **b**, Cells as in **a** were analysed by immunofluorescence (replicated three times) and quantified to calculate the percentage of cells showing TFEB nuclear localization. Scale bar, 10 µm. $n = 4$ independent fields per condition. **c**, Representative immunoblotting and quantification (mean ± s.e.m.; $n = 3$ experiments) of HeLa cells that stably express GFP–TFEB, transfected with the indicated siRNAs and subjected to amino acid starvation and refeeding (Methods) in the presence or absence of 250 nM torin. Plots on the right show pTFEB/TFEB (top), pS6K/S6K (middle) and p4E-BP1/GAPDH (bottom) ratios. siRHEB/L1, siRNA against *RHEB* and *RHEBL1*. **d**, Confocal microscopy analysis (replicated twice) of HeLa cells depleted for either RHEB and RHEBL1 (siRHEB/L1) or mTOR (siMTOR) and in control cells (siControl). Scale bar, 10 µm. The graph shows the percentage of cells showing TFEB nuclear localization. $n = 3$ independent fields per condition. **e**, HeLa cells transfected for 48 h with either *TSC2*-targeting (siTSC2) or control (siControl) siRNA were either left untreated, starved of amino acids for 60 min or treated with 250 nM torin for 60 min before immunoblotting analysis (replicated three times). **f**, Cells described in **e** were stained with TFEB antibodies, analysed by confocal microscopy (replicated three times) and quantified to calculate the percentage of cells that showed TFEB nuclear localization. Scale bar, 10 µm. Results are mean ± s.e.m. $n = 5$ independent fields per condition.

and 4E-BP1 (Fig. 1c, d, Extended Data Fig. 2a–d). Consistently, overexpression of RHEB had no effect on TFEB phosphorylation, but strongly induced the phosphorylation of S6K and 4E-BP1 in starved cells (Extended Data Fig. 2e). Furthermore, siRNA-mediated depletion of *TSC2* (a negative regulator of RHEB) did not affect the phosphorylation or subcellular localization of TFEB, which remained sensitive to amino acid deprivation (Fig. 1e, f). Conversely, knockdown of both RagC and RagD substantially impaired both TFEB phosphorylation and cytosolic localization (Extended Data Fig. 3a, b), which was equally rescued by re-expression of either RagC or RagD (Extended Data Fig. 3b). Thus, the phosphorylation of TFEB by mTORC1 is insensitive to perturbations of the TSC–RHEB axis (which is activated by growth factors) but highly sensitive to the amino-acid-dependent activation of Rag GTPases.

Rag GTPases mediate mTORC1–TFEB interaction

Next, we sought to identify the mechanism that underlies the different responses of TFEB and S6K or 4E-BP1 to mTORC1-activating stimuli. TFEB is known to interact with Rag GTPases, and this interaction is important for TFEB phosphorylation by mTORC1[26]. However, why mTORC1-mediated phosphorylation of TFEB requires its interaction with the Rag GTPases remains unclear, considering that none of the other mTORC1 substrates has been shown to interact with the Rag GTPases. Furthermore, our analysis of the TFEB protein sequence did not identify a TOR signalling (TOS) motif, a region that is known to mediate mTORC1 substrate recruitment through direct binding with regulatory-associated protein of mTOR (RAPTOR)[27,28]. Thus, we reasoned that the unconventional behaviour of TFEB phosphorylation by mTORC1 may be due to an alternative substrate-recruitment mechanism mediated by Rag GTPases. In vitro copurification revealed a direct interaction between recombinant TFEB and a Rag GTPase dimer composed of active RagA and RagC (RagA(Q66L) and RagC(S75N)) (Fig. 2a). Furthermore, co-immunoprecipitation experiments in HeLa cells revealed that TFEB interacts with Rag GTPases, RAPTOR and mTOR (Extended Data Fig. 4a), whereas no interaction of S6K with Rag GTPases was observed despite binding to both mTOR and RAPTOR (Extended Data Fig. 4b). Notably, we found that the interaction of mTORC1 with TFEB was considerably impaired in RagA and RagB double-knockout cells, and was restored upon reconstitution of these cells with wild-type RagA (Fig. 2b); by contrast, the absence of RagA and RagB did not affect

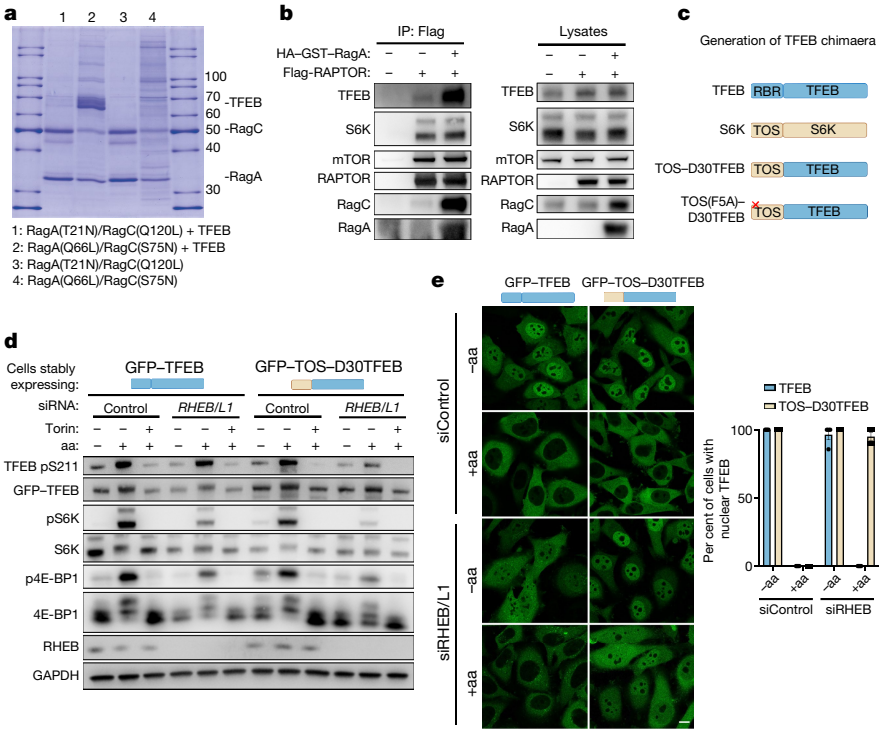

Fig. 2 | Unconventional recruitment of an mTORC1 substrate by Rag GTPases. a, Coomassie-stained gel of eluted size-exclusion chromatography fractions containing the different combinations of active and inactive Rag GTPases, in the presence or absence of TFEB. **b**, HEK293A cells deficient in RagA and RagB, and transfected with the indicated constructs, were lysed, incubated with Flag beads and analysed by immunoblotting (replicated three times). HA, haemagglutinin; GST, glutathione *S*-transferase; IP, immunoprecipitation. **c**, Schematic of TFEB chimeric constructs (Methods). RBR, Rag-binding region. TOS(F5A)–D30TFEB, a variant of the TOS–D30TFEB chimeric protein in which a key phenylalanine residue (F5) of the TOS motif was mutagenized to alanine. **d**, HeLa cells that stably express GFP–TFEB or the GFP–TOS–D30TFEB chimeric construct were transfected with either *RHEB/L1*-targeting or control siRNA, subjected to amino acid starvation and refeeding (Methods) in the presence or absence of 250 nM torin, and analysed by immunoblotting (replicated three times). **e**, Cells as in **d** were analysed by immunofluorescence (replicated three times) and quantified to calculate the percentage of cells that showed TFEB nuclear localization. Scale bar, 10 μm. Results are mean ± s.e.m. $n = 4$ independent fields per condition.

the interaction between mTORC1 and S6K (Fig. 2b). These data suggest that Rag GTPases are required for the interaction of mTORC1 with TFEB, whereas they are dispensable for its interaction with S6K.

The expression of a previously described construct (Lys–RAPTOR)—which promotes constitutive lysosomal recruitment and Rag-independent activation of mTORC1[13]—in cells silenced for both RagC and RagD rescued the phosphorylation of S6K and 4E-BP1 but was unable to rescue TFEB phosphorylation (Extended Data Fig. 4c, d), which indicates that mTORC1-mediated phosphorylation of TFEB requires Rag GTPases even in conditions that lead to the constitutive lysosomal localization of mTORC1. We obtained similar results by co-targeting both RAPTOR and RHEB to mitochondria using a previously described approach[29]; this resulted in constitutive phosphorylation of S6K and 4E-BP1, whereas TFEB phosphorylation and subcellular localization remained sensitive to nutrient availability (Extended Data Fig. 4e–g). These data suggest that, unlike S6K and 4E-BP1, the phosphorylation of TFEB requires active Rag GTPases, regardless of lysosomal localization and RHEB-induced activation of mTORC1.

We reasoned that substituting the first 30 amino acids of TFEB—which are required for the interaction of TFEB with Rag GTPases and for mTORC1-mediated phosphorylation[26] (Extended Data Figs. 5, 6a, b)—with the first 30 amino acids of S6K containing the TOS motif[27,28] (Fig. 2c) would change the phosphorylation behaviour of TFEB, making it similar to that of S6K. Consistent with our hypothesis, the resulting chimaera (TOS–D30TFEB) was able to interact with both mTOR and RAPTOR but not with Rag GTPases (Extended Data Fig. 5). Consequently, the phosphorylation and subcellular localization of TOS–D30TFEB became sensitive to serum starvation (Extended Data Fig. 6c–e) and RHEB/L1 depletion (Fig. 2d, e), in addition to amino acid deprivation (Extended Data Fig. 6a, b). Furthermore, unlike wild-type TFEB, TOS–D30TFEB did not localize to lysosomes in cells treated with torin (Extended Data Fig. 6b), which supports the idea that the lysosomal localization of TFEB is mediated by its interaction with Rag GTPases and not by an interaction with RAPTOR. Together, these data indicate that the differences in the phosphorylation behaviour of TFEB and S6K are not due to the intrinsic properties of the analysed phosphosites but are caused by different substrate-recruitment mechanisms, which define the specificity of mTORC1-mediated metabolic responses to diverse nutritional cues.

TFEB phosphorylation requires active RagC/D

Considering the absolute dependence of TFEB phosphorylation on Rag GTPases, we evaluated whether the activation of Rag GTPases has a differential role in the phosphorylation of TFEB versus S6K or 4E-BP1. As expected, expression of an active RagA(Q66L) mutant in RagA-knockout cells restored lysosomal localization of mTORC1 and promoted the cytoplasmic localization of TFEB, whereas inactive RagA(T21L) had no effect on either mTORC1 or TFEB localization (Extended Data Fig. 7). However, activation of RagC had a differential effect on the localization of mTORC1 and TFEB. Whereas only active RagC(S75L) induced the cytoplasmic localization of TFEB in RagC-knockout cells, both active RagC(S75L) and inactive RagC(Q120L) were able to significantly promote the lysosomal localization of mTORC1 (Fig. 3a–d, Extended Data Fig. 8a). Consistently, expression of active RagC(S75L) in RagC-knockout HeLa cells restored phosphorylation of TFEB, S6K and 4E-BP1 (Fig. 3e), whereas expression of inactive RagC(Q120L) was

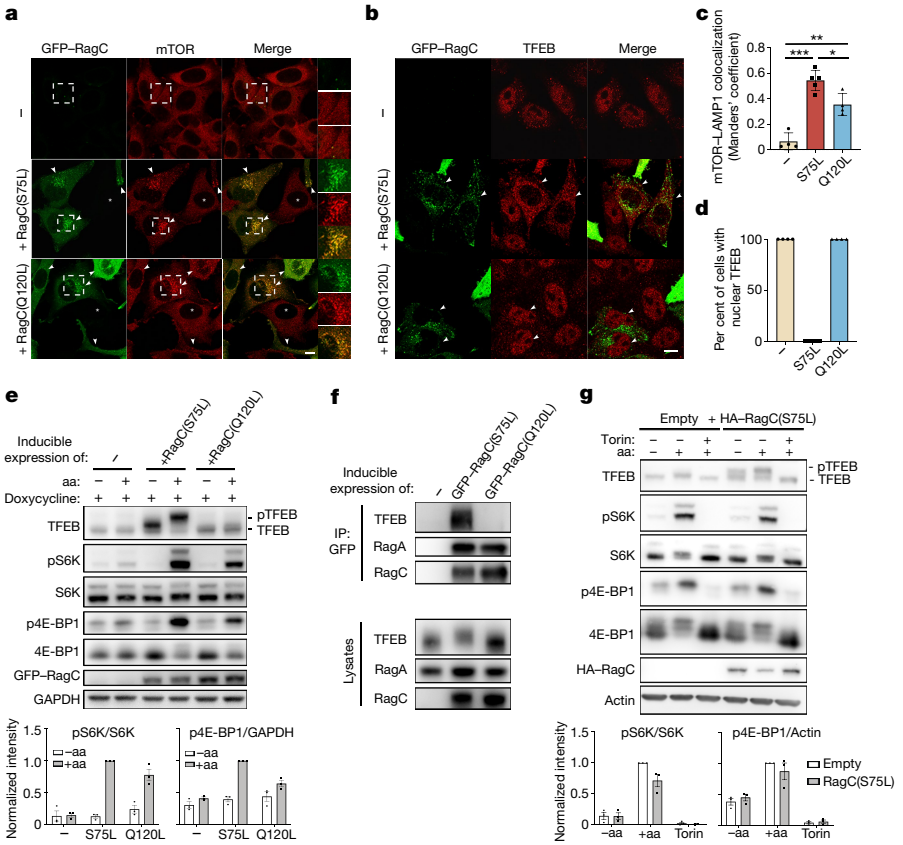

Fig. 3 | Activation of RagC has a differential effect on mTORC1 substrates. **a**, **b**, RagC-knockout HeLa cells with inducible expression of either active GFP–RagC(S75L) or inactive GFP–RagC(Q120L) were transfected for 24 h with siRNA targeting *RRAGD* (which encodes RagD), treated with doxycycline for additional 48 h, and then stained with mTOR (**a**) or TFEB (**b**) antibodies (replicated three times). Scale bar, 10 µm. **c**, Cells described in **a** were analysed for mTOR–LAMP1 colocalization by calculating Manders' colocalization coefficient. Results are mean ± s.d. $n = 4$ independent fields per condition. $^{*}P = 0.0119$, $^{**}P = 0.001$, $^{***}P < 0.0001$. Tukey's multiple comparisons test. **d**, Cells in **b** were quantified to calculate the percentage of cells that showed TFEB nuclear localization. $n = 4$ independent fields per condition. **e**, Cells as in **a** were subjected to amino acid starvation and refeeding (Methods), analysed by immunoblotting and quantified (mean ± s.e.m.; $n = 3$ experiments). Plots show pS6K/S6K (left) and p4E-BP1/GAPDH (right) ratios. **f**, Cell lysates from HEK293T cells with inducible expression of either active GFP–RagC(S75L) or inactive GFP–RagC(Q120L) were incubated with GFP beads and analysed by immunoblotting (replicated three times). **g**, Representative immunoblotting and quantification (mean ± s.e.m.; $n = 3$ experiments) of FLCN-knockout HeLa cells transfected with control vector (empty) or RagC(S75L) and subjected to amino acid starvation and refeeding, in the presence or absence of 250 nM torin. Plots show pS6K/S6K (left) and p4E-BP1/actin (right) ratios.

unable to rescue TFEB phosphorylation but was able to promote considerable phosphorylation of S6K and 4E-BP1 (Fig. 3e). Furthermore, co-immunoprecipitation experiments in HEK293T cells showed that TFEB was able to co-immunoprecipitate with active RagC(S75L) but unable to interact with inactive RagC(Q120L) (Fig. 3f).

Consistent with these data, cells that lack FLCN—a specific GTPase-activating protein for RagC/D[16–18]—showed phosphorylation of S6K and 4E-BP1 (Extended Data Fig. 8b), whereas TFEB was dephosphorylated and localized in the nucleus (Extended Data Fig. 8b, c). Importantly, expression of active RagC(S75L) or RagD(S77L) mutants in FLCN-knockout cells rescued TFEB phosphorylation (Fig. 3g, Extended Data Fig. 8d) and subcellular localization (Extended Data Fig. 8e, f). Together, these data suggest that a dimer of active RagA and inactive RagC is unable to promote mTORC1 activity towards TFEB, whereas it retains—to a large extent—its ability to promote mTORC1 lysosomal recruitment and consequent phosphorylation of S6K and 4E-BP1.

TFEB drives the kidney phenotype of BHD mice

On the basis of the previously described role of FLCN as a repressor of TFEB activity, we postulated that the kidney phenotype of individuals with BHD syndrome (a disease caused by loss-of-function mutations of *FLCN*[6,7]) is due to TFEB activation. To test this hypothesis, we generated mice with a kidney-specific double knockout of FLCN and TFEB (*Flcn*$^{flox/flox}$;*Tfeb*$^{flox/flox}$;*Ksp-cre*$^{+}$ mice; *Ksp* is also known as *Cdh16*)) (Extended Data Fig. 9) and compared their phenotype to previously described mice with kidney-specific knockout of *Flcn*[30,31].

Tfeb$^{flox/flox}$;*Ksp-cre*$^{+}$ mice were viable and fertile, and showed no apparent phenotypic abnormalities. As shown in previous reports[30,31], *Flcn*$^{flox/flox}$;*Ksp-cre*$^{+}$ mice presented enlarged kidneys that completely filled the abdominal cavity and were over twentyfold heavier than kidneys from control mice at post-natal day 21 (Fig. 4a–c). Histological analysis revealed severe polycystic disease, associated with intracystic accumulation of colloid-like material and pre-neoplastic lesions (Fig. 4d, Extended Data Fig. 10a). This phenotype was associated with a progressive increase in the level of blood urea nitrogen and in premature death before 30 days of life in all mice (Fig. 4e, f). Kidney samples from these mice also showed increased nuclear localization of TFEB (Extended Data Fig. 10b, c) and highly enhanced mTORC1 signalling, as measured by both immunofluorescence and immunoblotting; by contrast, AMPK signalling was not affected (Fig. 4g, Extended Data Fig. 10d). Finally, levels of RagC and RagD were increased, as were levels of previously described[25,32] TFEB targets (Extended Data Fig. 10d–f). The phenotype and associated signalling abnormalities of FLCN-knockout mice were completely reverted in the double-knockout mice, which were all indistinguishable from littermate controls without any instance

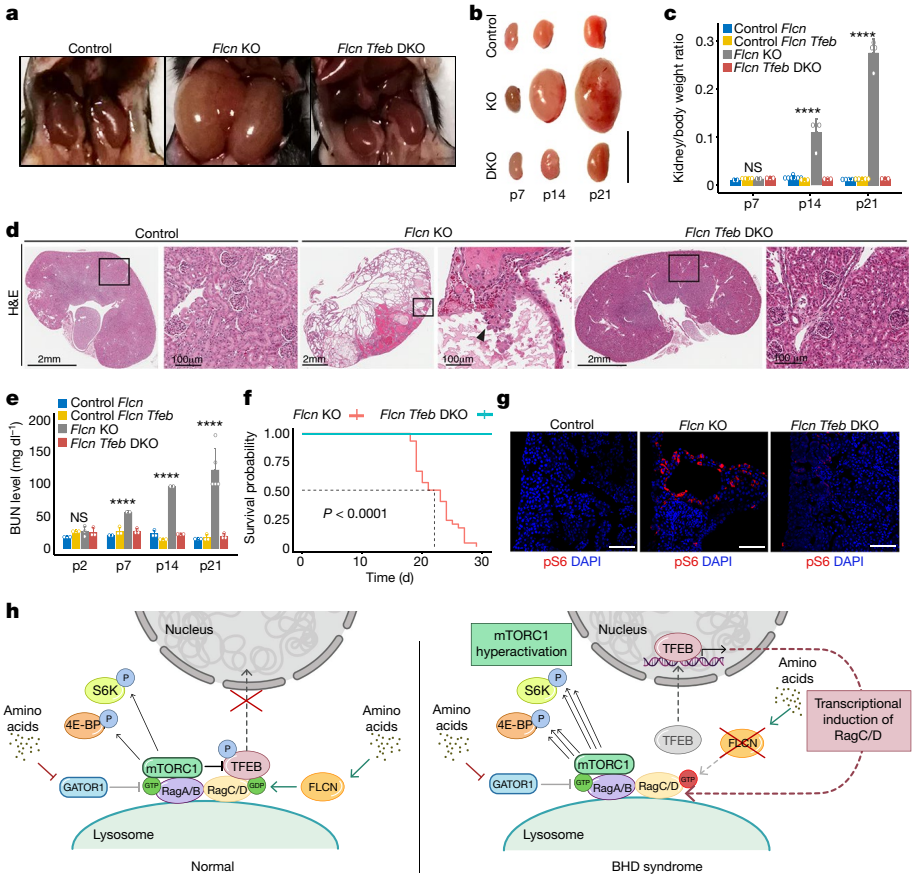

Fig. 4 | TFEB depletion rescues renal pathology and lethality in FLCN-knockout mice. a, Abdominal cavities of *Flcn*$^{flox/flox}$ (control), *Flcn*$^{flox/flox}$;*Ksp-cre*$^{+}$ (*Flcn* KO), and *Flcn*$^{flox/flox}$;*Tfeb*$^{flox/flox}$;*Ksp-cre*$^{+}$ (*Flcn Tfeb* DKO) mice at 21 day old. **b**, Pictures of kidneys from the *Flcn*$^{flox/flox}$ (top), *Flcn*$^{flox/flox}$;*Ksp-cre*$^{+}$ (middle) and *Flcn*$^{flox/flox}$;*Tfeb*$^{flox/flox}$;*Ksp-cre*$^{+}$ (bottom) mice at postnatal day (p)7, p14 and p21. Scale bar, 1 cm. **c**, Ratio of kidney to body weight for *Flcn*$^{flox/flox}$ mice (control *Flcn*) and *Flcn*$^{flox/flox}$;*Tfeb*$^{flox/flox}$ mice (control *Flcn Tfeb*), *Flcn*$^{flox/flox}$;*Ksp-cre*$^{+}$ (*Flcn* KO) and *Flcn*$^{flox/flox}$;*Tfeb*$^{flox/flox}$;*Ksp-cre*$^{+}$ (*Flcn Tfeb* DKO) at the indicated time-points. One-way analysis of variance was applied for each time point ($P = 0.14$ at p7, $P = 3.4 \times 10^{-7}$ at p14, $P = 9.3 \times 10^{-14}$ at p21). For P value < 0.05, a post hoc Tukey was applied; significance for each comparison is provided in Methods. At p7, $n = 3$ for control *Flcn*, *Flcn* KO and *Flcn Tfeb* DKO, and $n = 4$ for control *Flcn Tfeb*; at p14, $n = 7$ for control *Flcn*, $n = 4$ for *Flcn* KO and $n = 3$ for control *Flcn Tfeb* and *Flcn Tfeb* DKO; at p21, $n = 6$ for control *Flcn*, $n = 4$ for *Flcn* KO, $n = 5$ for control *Flcn Tfeb* and $n = 3$ for *Flcn Tfeb* DKO. Error bars represent s.d. **d**, Haematoxylin and eosin staining (H & E) of kidneys from *Flcn* KO, *Flcn Tfeb* DKO and control mice at p21 (replicated three times). Scale bars, 2 mm (left panels). Boxed areas are magnified on the right. Arrowhead indicates tubular papillary atypical hyperplasia. Scale bars, 100 μm (right panels). **e**, Blood urea nitrogen (BUN) levels of mice of the indicated genotypes at the indicated time points. Statistics were applied as in **c** ($P = 0.23$ at p2, $P = 1.2 \times 10^{-5}$ at p7, $P = 1.9 \times 10^{-9}$ at p14, $P = 6.4 \times 10^{-4}$ at p21), $n = 3$ mice for each genotype and time point. Error bars represent s.d. **f**, Kaplan–Meyer survival analysis of *Flcn* KO ($n = 30$) and *Flcn Tfeb* DKO ($n = 29$) mice. Two-sided log–rank test, $P < 0.0001$. The median survival time (dashed line) of the *Flcn*-KO group is 22 d. **g**, Immunofluorescence of pS6 in kidney sections from mice of the indicated genotypes (replicated three times). Scale bars, 100 μm. **h**, Model illustrating differential regulation of mTORC1 substrates in normal conditions (left), and in BHD syndrome (right). The activation of Rag GTPases by amino acids leads to phosphorylation of S6K, 4E-BP1 and TFEB, which is retained in the cytoplasm. In BHD syndrome, the loss of function of FLCN leads to the nuclear translocation of TFEB and hyperactivation of mTORC1.

of premature lethality at up to 10 months of observation (Fig. 4f). These mice showed normal kidney size, morphology and histology, as well as normal blood urea nitrogen values and mTORC1 activity (Fig. 4 a–e, g, Extended Data Fig. 10d). These results suggest that the constitutive activation of TFEB as a result of the loss of function of FLCN is a crucial determinant of the kidney phenotype associated with BHD syndrome.

Discussion

Here we show that diversity in mTORC1 substrate-recruitment mechanisms between TFEB and S6K or 4E-BP1 enables selective metabolic responses to specific nutritional inputs (such as amino acids and growth factors). The insensitivity of mTORC1-mediated phosphorylation of TFEB to the growth-factor-driven TSC–RHEB axis raises the question of how mTORC1 might be activated in the absence of RHEB. It is possible that the conformational change induced by RHEB, which acts as an allosteric activator of mTORC1[11], may favour accessibility and catalysis of some specific mTOR substrates (such as S6K and 4E-BP1) and may not be needed for others (such as TFEB).

Our data also indicate that the activity of FLCN, an activator of RagC/D, is crucial for the mTORC1-mediated phosphorylation of TFEB. By contrast, FLCN is largely dispensable for the phosphorylation of S6K and 4E-BP1, consistent with previous studies[17,33]. Our finding that inactive RagC is incapable of binding TFEB but is able to promote the lysosomal recruitment of mTORC1 (Fig. 3) provides a mechanistic explanation for these observations. These findings are consistent with recent structural data that show that the interaction of mTORC1 with the RagA–RagC dimer is largely mediated by the interaction between RAPTOR and RagA, whereas the nucleotide-binding state of RagC has a lesser contribution towards RAPTOR recruitment[34,35].

Overexpression of genes belonging to the MiT-TFE family, such as *TFEB*, leads to kidney cysts and renal cell carcinoma both in humans and mice[36–38], a phenotype that is notably similar to that caused by loss of FLCN[6]. This prompted us to investigate whether the loss of function of

TFEB rescued the phenotype of mice with kidney-specific knockout of FLCN. Genetic depletion of *Tfeb* resulted in a complete rescue of renal cyst formation and precancerous lesions, restoring normal kidney function and viability of mice with kidney-specific knockout of FLCN (Fig. 4). This suggests that TFEB activation is a key driver of the kidney phenotype of individuals with BHD syndrome; whether or not TFEB also has a role in other clinical manifestations of BHD syndrome (which affect organs other than the kidney) will be the subject of future studies.

BHD syndrome is associated with the hyperactivation of mTORC1[30,31,39]. This raises the question of how the loss of function of FLCN, which is a positive regulator of mTORC1[16,40], can lead to mTORC1 hyperactivity. We found no major changes in the activity of AMPK, which is a negative regulator of mTORC1 and interacts with the FLCN–FNIP complex[39], in the kidneys from FLCN-knockout mice compared to control mice (Extended Data Fig. 10d). It has previously been reported that TFEB promotes mTORC1 activity by transcriptionally regulating the levels of RagC and RagD GTPases[25]. Here we show that the constitutive activation of TFEB in FLCN-knockout mice results in increased expression of RagC and RagD GTPases (Extended Data Fig. 10d, e), which—although inactive in the absence of FLCN—are able to promote mTORC1 activity on S6K and 4E-BP1 but not on TFEB (Fig. 3), thus explaining the paradox of mTORC1 hyperactivity in BHD syndrome. Although our data suggest that hyperactivity of mTORC1 induced by TFEB is a key step in kidney cystogenesis and tumorigenesis, we cannot rule out the possibility that the upregulation of other TFEB-induced pathways may also contribute to the phenotype of BHD syndrome. Increased glycogenesis has previously been reported in mice with muscle-specific overexpression of TFEB[41]; similar findings have been reported in mice with conditional and kidney-specific knockout of FLCN[42,43], suggesting that this pathway—which is downstream of FLCN and TFEB—may be an additional mechanism that contributes to BHD syndrome.

In summary, our study identifies a substrate-specific mTORC1 pathway that promotes kidney cystogenesis and tumorigenesis (Fig. 4h). Other types of malignancies have been shown to be associated with high levels of MiT-TFE factors and concomitant mTORC1 hyperactivation[25,44], which suggests that targeting this regulatory pathway may represent a promising therapeutic strategy for a variety of cancers.

Online content

Any methods, additional references, Nature Research reporting summaries, source data, extended data, supplementary information, acknowledgements, peer review information; details of author contributions and competing interests; and statements of data and code availability are available at https://doi.org/10.1038/s41586-020-2444-0.

1. Liu, G. Y. & Sabatini, D. M. mTOR at the nexus of nutrition, growth, ageing and disease. *Nat. Rev. Mol. Cell Biol.* **21**, 183–203 (2020).
2. Ben-Sahra, I. & Manning, B. D. mTORC1 signaling and the metabolic control of cell growth. *Curr. Opin. Cell Biol.* **45**, 72–82 (2017).
3. González, A. & Hall, M. N. Nutrient sensing and TOR signaling in yeast and mammals. *EMBO J.* **36**, 397–408 (2017).
4. Sardiello, M. et al. A gene network regulating lysosomal biogenesis and function. *Science* **325**, 473–477 (2009).
5. Settembre, C. et al. TFEB links autophagy to lysosomal biogenesis. *Science* **332**, 1429–1433 (2011).
6. Schmidt, L. S. & Linehan, W. M. *FLCN*: the causative gene for Birt–Hogg–Dubé syndrome. *Gene* **640**, 28–42 (2018).
7. Schmidt, L. S. & Linehan, W. M. Molecular genetics and clinical features of Birt–Hogg–Dubé syndrome. *Nat. Rev. Urol.* **12**, 558–569 (2015).
8. Inoki, K., Li, Y., Xu, T. & Guan, K. L. Rheb GTPase is a direct target of TSC2 GAP activity and regulates mTOR signaling. *Genes Dev.* **17**, 1829–1834 (2003).
9. Long, X., Lin, Y., Ortiz-Vega, S., Yonezawa, K. & Avruch, J. Rheb binds and regulates the mTOR kinase. *Curr. Biol.* **15**, 702–713 (2005).
10. Tee, A. R., Manning, B. D., Roux, P. P., Cantley, L. C. & Blenis, J. Tuberous sclerosis complex gene products, tuberin and hamartin, control mTOR signaling by acting as a GTPase-activating protein complex toward Rheb. *Curr. Biol.* **13**, 1259–1268 (2003).
11. Yang, H. et al. Mechanisms of mTORC1 activation by RHEB and inhibition by PRAS40. *Nature* **552**, 368–373 (2017).
12. Sancak, Y. et al. The Rag GTPases bind raptor and mediate amino acid signaling to mTORC1. *Science* **320**, 1496–1501 (2008).
13. Sancak, Y. et al. Ragulator–Rag complex targets mTORC1 to the lysosomal surface and is necessary for its activation by amino acids. *Cell* **141**, 290–303 (2010).
14. Kim, E., Goraksha-Hicks, P., Li, L., Neufeld, T. P. & Guan, K. L. Regulation of TORC1 by Rag GTPases in nutrient response. *Nat. Cell Biol.* **10**, 935–945 (2008).
15. Bar-Peled, L. et al. A tumor suppressor complex with GAP activity for the Rag GTPases that signal amino acid sufficiency to mTORC1. *Science* **340**, 1100–1106 (2013).
16. Tsun, Z. Y. et al. The folliculin tumor suppressor is a GAP for the RagC/D GTPases that signal amino acid levels to mTORC1. *Mol. Cell* **52**, 495–505 (2013).
17. Lawrence, R. E. et al. Structural mechanism of a Rag GTPase activation checkpoint by the lysosomal folliculin complex. *Science* **366**, 971–977 (2019).
18. Shen, K. et al. Cryo-EM structure of the human FLCN–FNIP2–Rag–Ragulator complex. *Cell* **179**, 1319–1329.e8 (2019).
19. Settembre, C. et al. A lysosome-to-nucleus signalling mechanism senses and regulates the lysosome via mTOR and TFEB. *EMBO J.* **31**, 1095–1108 (2012).
20. Martina, J. A., Chen, Y., Gucek, M. & Puertollano, R. MTORC1 functions as a transcriptional regulator of autophagy by preventing nuclear transport of TFEB. *Autophagy* **8**, 903–914 (2012).
21. Roczniak-Ferguson, A. et al. The transcription factor TFEB links mTORC1 signaling to transcriptional control of lysosome homeostasis. *Sci. Signal.* **5**, ra42 (2012).
22. Napolitano, G. et al. mTOR-dependent phosphorylation controls TFEB nuclear export. *Nat. Commun.* **9**, 3312 (2018).
23. Medina, D. L. et al. Lysosomal calcium signalling regulates autophagy through calcineurin and TFEB. *Nat. Cell Biol.* **17**, 288–299 (2015).
24. Ballabio, A. & Bonifacino, J. S. Lysosomes as dynamic regulators of cell and organismal homeostasis. *Nat. Rev. Mol. Cell Biol.* **21**, 101–118 (2019).
25. Di Malta, C. et al. Transcriptional activation of RagD GTPase controls mTORC1 and promotes cancer growth. *Science* **356**, 1188–1192 (2017).
26. Martina, J. A. & Puertollano, R. Rag GTPases mediate amino acid-dependent recruitment of TFEB and MITF to lysosomes. *J. Cell Biol.* **200**, 475–491 (2013).
27. Schalm, S. S. & Blenis, J. Identification of a conserved motif required for mTOR signaling. *Curr. Biol.* **12**, 632–639 (2002).
28. Schalm, S. S., Fingar, D. C., Sabatini, D. M. & Blenis, J. TOS motif-mediated raptor binding regulates 4E-BP1 multisite phosphorylation and function. *Curr. Biol.* **13**, 797–806 (2003).
29. Lawrence, R. E. et al. A nutrient-induced affinity switch controls mTORC1 activation by its Rag GTPase–Ragulator lysosomal scaffold. *Nat. Cell Biol.* **20**, 1052–1063 (2018).
30. Baba, M. et al. Kidney-targeted Birt–Hogg–Dubé gene inactivation in a mouse model: Erk1/2 and Akt–mTOR activation, cell hyperproliferation, and polycystic kidneys. *J. Natl. Cancer Inst.* **100**, 140–154 (2008).
31. Chen, J. et al. Deficiency of FLCN in mouse kidney led to development of polycystic kidneys and renal neoplasia. *PLoS ONE* **3**, e3581 (2008).
32. Palmieri, M. et al. Characterization of the CLEAR network reveals an integrated control of cellular clearance pathways. *Hum. Mol. Genet.* **20**, 3852–3866 (2011).
33. Wada, S. et al. The tumor suppressor FLCN mediates an alternate mTOR pathway to regulate browning of adipose tissue. *Genes Dev.* **30**, 2551–2564 (2016).
34. Anandapadamanaban, M. et al. Architecture of human Rag GTPase heterodimers and their complex with mTORC1. *Science* **366**, 203–210 (2019).
35. Rogala, K. B. et al. Structural basis for the docking of mTORC1 on the lysosomal surface. *Science* **366**, 468–475 (2019).
36. Kauffman, E. C. et al. Molecular genetics and cellular features of TFE3 and TFEB fusion kidney cancers. *Nat. Rev. Urol.* **11**, 465–475 (2014).
37. Calcagnì, A. et al. Modelling TFE renal cell carcinoma in mice reveals a critical role of WNT signaling. *eLife* **5**, e17047 (2016).
38. Perera, R. M., Di Malta, C. & Ballabio, A. MiT/TFE family of transcription factors, lysosomes, and cancer. *Annu Rev Cancer Biol* **3**, 203–222 (2019).
39. Baba, M. et al. Folliculin encoded by the *BHD* gene interacts with a binding protein, FNIP1, and AMPK, and is involved in AMPK and mTOR signaling. *Proc. Natl Acad. Sci. USA* **103**, 15552–15557 (2006).
40. Petit, C. S., Roczniak-Ferguson, A. & Ferguson, S. M. Recruitment of folliculin to lysosomes supports the amino acid-dependent activation of Rag GTPases. *J. Cell Biol.* **202**, 1107–1122 (2013).
41. Mansueto, G. et al. Transcription factor EB controls metabolic flexibility during exercise. *Cell Metab.* **25**, 182–196 (2017).
42. Endoh, M. et al. A FLCN–TFE3 feedback loop prevents excessive glycogenesis and phagocyte activation by regulating lysosome activity. *Cell Rep.* **30**, 1823–1834 (2020).
43. Possik, E. et al. FLCN and AMPK confer resistance to hyperosmotic stress via remodeling of glycogen stores. *PLoS Genet.* **11**, e1005520 (2015).
44. Perera, R. M. et al. Transcriptional control of autophagy–lysosome function drives pancreatic cancer metabolism. *Nature* **524**, 361–365 (2015).

Methods

No statistical methods were used to predetermine sample size. For animal experiments, mice of the same genotype were randomly assigned to different treatment groups. Investigators were blinded for immunofluorescence analyses.

Materials

Reagents used in this study were obtained from the following sources: antibodies to RagC (cat. no. 3360 - 1:1,000 WB), RagA (cat. no. 4357 - 1:1,000 WB), RagD (cat. no. 4470 - 1:1,000 western blot (WB)) mTOR (cat. no. 2983 - 1:1,000 WB/1:100 immunofluorescence (IF)) phospho-p70 S6 kinase (Thr389) (1A5) (cat. no. 9206 - 1:1,000 WB), p70 S6 kinase (cat. no. 9202 - 1:1,000 WB), RHEB1 (cat. no. 13879 - 1:1,000 WB), 4E-BP1 (cat. no. 9644 - 1:1,000 WB), phospho-4E-BP1 (Ser65) (cat. no. 9456 - 1:1,000 WB), RPTOR (24C12) (cat. no. 2280 - 1:1,000 WB), human TFEB (cat. no. 4240 - 1:1,000 WB/1:100 IF), tuberin/TSC2 (cat. no. 4308 - 1:1,000 WB), FLCN (cat. no. 3697 - 1:1,000 WB), phospho-ULK1 (cat. no. 6888 - 1:1,000 WB), pan-ULK1 (cat. no. 8054 - 1:1,000 WB), phospho-AMPK (T172) (cat. no. 2535 - 1:1,000 WB), anti-AMPK (cat. no. 2532 - 1:1,000 WB), phospho-S6 (cat.no.5364-1:100 IF) and Myctag (cat.no.2276-1:1,000 WB) were from Cell Signaling Technology; antibody to GFP (cat. no. ab13970 1:2,000 WB) was from Abcam; antibodies to GAPDH (6C5) (cat. no. sc-32233 - 1:15,000 WB), LAMP1 (H4A3) (cat. no. sc-20011 - 1:500 IF), LAMP1 (1D4B) (cat. no. sc-19992 - 1:200 immunohistochemistry (IHC)), lamin B (cat. no. sc-6216 - 1:1,000 WB) were from Santa Cruz; antibodies to Flag M2 (cat. no. F1804 - 1:1,000 WB) and actin (#A2228 - 1:5,000 WB) were from Sigma Aldrich; antibody to HA.11 epitope tag (cat. no. 901513 - 1:1,000 WB) was from Biolegend; antibody to mouse TFEB (cat. no. A303-673A - 1:1,000 WB/1:200 IF) and RagD (A304-301A - 1:1,000 WB) was from Bethyl laboratories; HRP-conjugated secondary antibodies to mouse (cat. no. 401215 - 1:5,000 dilution) and rabbit (cat. no. 401315 - 1:5,000 dilution) IgGs were from Calbiochem; donkey anti-rabbit IgG (H+L) Alexa Fluor 488 (cat. no. A-21206 - 1:500 dilution), Alexa Fluor 568 (cat. no. A-10042 - 1:500 dilution), donkey anti-mouse IgG (H+L) Alexa Fluor 568 (cat. no. A-10037 - 1:500 dilution), Alexa Fluor 647 (cat. no. A-31571 - 1:500 dilution), Alexa Fluor 594 (cat. no. A-21203 - 1:500 dilution), donkey anti-goat IgG (H+L) Alexa Fluor 647 (cat. no. A-21447 - 1:500 dilution) were from Thermo Fisher Scientific; antibodies to TFEB-pS211 (used at 1:1,000 WB) were custom-generated in collaboration with Bethyl Laboratories.

The chemicals used were torin 1 (cat. no. 4247) from Tocris; protease inhibitor cocktail (cat. no. P8340) and puromycin (cat. no. P9620) from Sigma Aldrich; and PhosSTOP phosphatase inhibitor cocktail tablets (cat. no. 04906837001) from Roche.

Cell cultures

Cells were cultured in the following media: HeLa in MEM (cat. no. ECB2071L, Euroclone); HEK 293T, HEK293A and MEFs in DMEM high glucose (cat. no. ECM0728L, Euroclone); U2OS in McCoy (cat. no. 26600, Gibco); ARPE19 in DMEM-F12 (cat. no. 11320033, Thermo Fisher Scientific). All media were supplemented with 10% inactivated FBS (cat. no. ECS0180L, Euroclone), 2 mM glutamine (cat. no. ECB3000D, Euroclone), penicillin (100 IU/ml) and streptomycin (100 µg/ml) (cat. no. ECB3001D, Euroclone) and maintained at 37 °C and 5% CO_2. RagA and RagB double-knockout (RagA/B-KO) and control HEK293A cells were kindly provided by K.-L. Guan. FLCN-knockout HeLa cells were a kind gift of Z. P. Arany. HeLa cells stably expressing TFEB–GFP have previously been described[19]. Cell lines stably expressing TFEB–GFP, TFEB(Δ30)–TOS –GFP and S6K–GFP were generated using the Tol2 system as previously described[45]. RagC-KO HeLa cells or HEK293T cells with inducible expression of either active or inactive RagC were generated upon transduction of these cells with pLVX-TETONE-GFP-RagC-S75L and pLVX-TETONE-GFP-RagC-Q120L inducible lentiviral plasmids.

All cell lines were purchased from ATCC, validated by morphological analysis and routinely tested for absence of mycoplasma.

Derivation of primary mouse embryonic fibroblasts (MEFs)

Primary MEFs were derived from pregnant mice at embryonic day (E)13.5. Embryos were washed in phosphate–buffered saline (PBS) and dissected by removing their placenta, head, limbs and gonads, tail and other visceral mass. Cells were then isolated by mechanical activity (chopping the tissue into fine pieces) and cultured in DMEM supplemented with 10% inactivated FBS, glutamine and antibiotics.

Generation of *RRAGA* and *RRAGC* knockout in HeLa cell lines

In HeLa cells, full knockout of the *RRAGA* and *RRAGC* genes was generated using the CRISPR–Cas9 system. The guide (g)RNA sequences for each gene with low off-target score were selected using the http://crispor.tefor.net/crispor.py online tool. One gRNA was selected for each gene: CTCCCACGTCCGATTCCTA for the *RRAGA* gene and TCATGGGACTCCGGCGCAG for the *RRAGC* gene. The 'ALL in One' vector containing each gRNA was obtained from Sigma (CAS9GFPP). HeLa cells were electroporated using the Amaxa system with the nucleofection kit (cat. no. VCA-1003 from Lonza). GFP-positive cells were FACS-sorted into 96-well plates to obtain single-cell-derived colonies carrying the indel mutations. Upon genomic DNA extraction, the genomic sequence containing the targeted region was amplified by PCR reaction with the specific primers: human *RRAGA* knockout up TGCTGCTGATGGGGAAGAG, human *RRAGA* knockout low TTTGGCGTCAGGAGAGTTCT, human *RRAGC* knockout up GCCGATTCGTTTCCAAAGGA, and human *RRAGC* knockout low AGTGGAAGAGAAAGTGCGGA. PCR products were analysed by DNA Sanger sequencing and cell clones carrying homozygous mutations introducing a premature stop codon (c.156DELc and c.196DELtcatgggactccggcgc for the *RRAGA* and *RRAGC* genes, respectively) were selected and expanded.

Plasmids

The plasmid encoding full-length TFEB–GFP has previously been described[23]. pLJM1-Flag-Raptor wt (no. 26633), pLJM1-Flag-Raptor-RHEB15 (no. 26634), pRK5-HA GST RagA-Q66L (no. 19300), pRK5-HA GST RagA-T21L (no. 19299), pRK5-HA GST RagC-S75L (no. 19305) and pRK5-HA GST RagC-Q120L (no. 19306) were a kind gift from D. Sabatini (Addgene plasmids). pcDNA3-Flag-RHEB (no. 19996) was a gift from F. Tamanoi (Addgene plasmid). pEGFP-N1-delta30-TFEB was a gift from S. Ferguson (Addgene plasmid no. 44445). pLVX-TETONE-GFP-RagC-S75L and pLVX-TETONE-GFP-RagC-Q120L inducible lentiviral plasmids were generated by standard cloning using the In-fusion HD cloning kit (no. 638920, Takara). pRK5-Flag-Raptor-OMP25 (mitochondrially targeted (Mit-)Raptor) and pRK5-Myc-RHEB-OMP25 plasmids were a kind gift from R. Zoncu. Tol2 plasmids for expression of TFEB–GFP, TOS–D30TFEB–GFP and S6K–GFP were generated by standard cloning. TOS(F5A)–D30TFEB–GFP was generated by using QuikChange II-E Site-Directed Mutagenesis Kit (no. 200555, Agilent Technologies).

Cell treatments and protein knockdown

For experiments involving amino acid starvation, cells were rinsed twice with PBS and incubated for 60 min (unless stated otherwise) in amino acid-free RPMI (cat. no. R9010-01, USBiological) or DMEM (cat. no. MBS6120661) supplemented with 10% dialysed FBS. Serum was dialysed against 1× PBS through 3,500-molecular weight cut-off dialysis tubing to ensure absence of contaminating amino acids. For amino acid refeeding, cells were re-stimulated for 30 min with 1× water-solubilized mix of essential (cat. no.11130036, Thermo Fisher Scientific) and non-essential (cat. no. 11140035, Thermo Fisher Scientific) amino acids resuspended in amino-acid-free RPMI or DMEM supplemented with 10% dialysed FBS, plus glutamine. For serum starvation, cells were washed twice with PBS, incubated with culture medium containing 10% dialysed FBS for 16 h, then washed twice with PBS and incubated with FBS-free culture

medium for the indicated time points. Where reported, cells were incubated with 250 nM torin 1 during either starvation or restimulation.

For siRNA-based experiments, cells were transfected using Lipofectamine RNAiMAX Transfection Reagent (no. 13778, Invitrogen) with the indicated siRNA and analysed after 72 h unless stated otherwise. The following siRNAs were used: siRNA *RHEB* I (no. 14267), siRNA *MTOR* I (no. 6381), siRNA *MTOR* II (no. 6556) were from Cell Signaling; human *RRAGD* siRNA (L-016120-00) and non-targeting siRNA pool (D-001810-10-05) were from Dharmacon. Other siRNA included *RHEBL1* siRNA: GAUAGUGACUCUUGGCAAA; *TSC2* siRNA: GCUGUUACCUCGACGAGUA; *RRAGC* siRNA: GUCUGAU GAUCACAAAAUA; GGAGCAUUGAUAUACGUCA; CAACUUCCACUGUUU CCGA, and were synthesized by Sigma Aldrich.

Mammalian lentiviral production and transduction

Lentiviruses were produced by transfection of HEK293T cells with pLJM1 Flag-Raptor-RHEB15, pLVX-TETONE-RagC-S75L or pLVX-TETONE-RagC-Q120L constructs in combination with the pCMV-VSV-G and pCMV-ΔR8.2 packaging plasmids using Lipofectamine 2000 transfection reagent (Invitrogen). Five hours after transfection, medium was changed to DMEM supplemented with 10% FBS. Forty-eight hours later, virus-containing supernatants were collected, passed through a 0.45-µm filter to eliminate cell debris and used for infection in the presence of 5 µg/ml polybrene (cat. no. tr-1003-G, EMD Millipore). Twenty-four hours later, cells were selected with puromycin.

Cell lysis, western blotting and immunoprecipitation

Cells were rinsed once with PBS and lysed in ice-cold lysis buffer (250 mM NaCl, 1% Triton, 25 mM Hepes pH 7.4) supplemented with protease and phosphatase inhibitors. Total lysates were passed 10 times through a 25-gauge needle with syringe, kept at 4 °C for 10 min and then cleared by centrifugation in a microcentrifuge (14,000 rpm at 4 °C for 10 min). Protein concentration was measured by Bradford assay.

For immunoprecipitations, cells grown in 10-cm culture dishes were washed twice with cold PBS and then incubated with 1 mg/ml DSP (dithiobis(succinimidyl propionate)) (cat. no.22586, Thermo Fischer Scientific) crosslinker for 7 min at room temperature. The crosslinking reaction was quenched by adding Tris-HCl (pH 8.5) to a final concentration of 100 mM. Cells were rinsed twice with ice cold PBS and lysed with RIPA lysis buffer (40 mM Hepes pH 7.4, 2mM EDTA, 1% NP-40, 1% sodium deoxycholate and 0.1% SDS) supplemented with protease and phosphatase inhibitors. Cell lysates were then incubated with anti-GFP trap agarose beads (cat. no. gta-20, Chromotek) or M2-Flag beads (Sigma) at 4 °C, washed 6 times, resolved by SDS-polyacrylamide gel electrophoresis on 4–12% Bis-Tris gradient gels (cat. no. NP0323PK2 NuPage, Thermo Fischer Scientific) and analysed by immunoblotting with the indicated primary antibodies.

Quantification of western blotting was performed by calculating the intensity of phosphorylated and total proteins by densitometry analysis using the Fiji software. The ratios between the values of phosphorylated and total proteins were normalized to a control condition for each experiment.

Generation of constructs for recombinant expression of RagA–RagC–TFEB and derived mutants

Secondary structure prediction highlighted that TFEB is predominantly disordered, with the exceptions of the N-terminal region, the helix–loop–helix and the leucine zipper domains present in the centre of the protein. To stabilize full-length TFEB during expression and purification, we have developed a strategy in which TFEB and the Rag GTPases are simultaneously expressed. We used the LAMTOR–RagA–RagC baculoviral construct previously described[46] and subcloned the codon-optimized *RRAGA* (Q7L523.1), and *RRAGC* (Q9HB90.1) open reading frames (ORFs) flanked by individual promoter and terminator signals into pACEBac1. An N-terminal 6×histidine tag was subsequently introduced upstream of the *RRAGA* ORF. We designed a synthetic gene corresponding to the *TFEB* ORF (P19484) tagged C-terminally with tandem Strep, codon-optimized for expression in *Spodoptera frugiperda* and flanked by unique restriction sites. The *TFEB* insert was chemically synthesized by GeneArt AG, Life Technologies and was then subcloned into the multiple cloning site of the pACEBac1 acceptor vector containing RagA–RagC.

The RagA(Q66L)–RagC(S75N)–TFEB and RagA(T21N)–RagC(Q120L)–TFEB were generated by site-directed mutagenesis using the above-described construct as template.

Protein expression and purification

The initial recombinant baculoviruses were amplified and used for induction of protein expression by infecting cells at a density of 0.5–1.0 × 10^6 cells per ml. Infection was performed with amplified virus stock at a multiplicity of infection (MOI) >1. Seventy-two to 96 h after infection, cells were collected by centrifugation, washed in PBS and drained pellets were frozen in liquid nitrogen and stored at −80 °C until use. In brief, complexes were purified by metal chelate affinity purification followed by size-exclusion chromatography (SEC). The cell pellet was resuspended in lysis buffer containing 50 mM Tris pH 8.0, 300 mM NaCl, 2 mM $MgCl_2$, 0.5 mM TCEP, 0.05% triton X-100 and 20 mM imidazole and flash-frozen in liquid nitrogen. After thawing the cells, the lysate was supplemented with protease inhibitors and cleared by centrifugation at 16,000*g* and 4 °C for 30 min. For the control samples, the obtained lysates were bound to a STREP-TRAP column to remove all TFEB and any associated Rag GTPases before the subsequent steps. The flow-through of these samples was then added to equilibrated Ni-NTA beads and incubated at 4 °C for 2.5 h on a rotating wheel. Beads were washed with 30 times the bead volume of lysis buffer and eluted in 50 mM Tris pH 8.0, 300 mM NaCl, 2 mM $MgCl_2$, 0.5 mM TCEP, 0.05% triton X-100 and 250 mM imidazole. The sample was immediately loaded on a Superdex 200 prep column equilibrated in 50 mM Tris pH 8.0, 300 mM NaCl, 2 mM $MgCl_2$, 0.5 mM TCEP, 0.05% triton X-100. The fractions containing the Rag GTPases–TFEB complex were pooled, concentrated, analysed by SDS–PAGE and visualized by Coomassie.

Kidney nuclear and cytosolic fractionation

Kidneys were homogenized by using a tissue grind pestle in cytosol isolation buffer (250 mM sucrose, 20 mM HEPES, 10 mM KCl, 1.5 mM MgCl2, 1 mM EDTA and 1 mM EGTA) supplemented with protease and phosphatase inhibitor cocktails (Complete and PhosSTOP Roche, Roche Diagnostics). Then samples were centrifuged at 1,000*g* for 10 min at 4 °C to pellet the nuclei and the supernatant (cytosolic fraction) recentrifuged twice at 16,000*g* for 20 min at 4 °C to pellet the mitochondria and debris. Nuclei pellets were washed with PBS and centrifuged at 800*g* for 10 min 3 times, then resuspended in nuclear lysis buffer (1.5 mM MgCl2, 0.2 mM EDTA, 20 mM HEPES, 0.5 M NaCl, 20% glycerol, 1% triton X-100) supplemented with protease and phosphatase inhibitor cocktails and incubated on ice for 30 min (vortexed every 10 min) and then sonicated 5 frequency about 10 s (for 3 times). Finally, samples were centrifuged for 15 min at 16,000*g* and the supernatant containing the enriched nuclear fraction collected.

Confocal microscopy

Immunofluorescence experiments were performed as previously described[47]. Cells were grown on 8-well Lab-Tek II - Chamber Slides, treated as indicated and fixed with 4% parafolmaldehyde (PFA) for 10 min at room temperature. Blocking was performed with 3% bovine serum albumin in PBS + 0.02% saponin for 1 h at room temperature. For endogenous TFEB staining, cells were also permeabilized with 0.1% triton X-100 for 5 min after PFA fixation and before blocking solution incubation to allow visualization of the nuclear signal. Immunostainings were performed upon dilution of primary antibodies in blocking

solution and overnight incubation at 4 °C, followed by three washes and secondary antibody incubation in blocking solution for 1 h at room temperature. After additional three washes, coverslips were finally mounted in VECTASHIELD mounting medium with DAPI and analysed using LSM 800 or LSM 880+ Airyscan systems (Carl Zeiss), with a Plan-Apochromat 63×/1.4 NA M27 oil immersion objective using immersion oil (no. 518F, Carl Zeiss) at room temperature. The microscopes were operated on the ZEN 2013 software platform (Carl Zeiss). After calculation of processing for the airyscan, images were processed in ImageJ v.1.47. Mander's colocalization coefficients was calculated using the JACoP ImageJ plugin.

For analysis of nuclear/cytosolic TFEB ratios, a dedicated script was developed using the Columbus software (Perkin-Elmer). The script calculates the ratio value resulting from the average intensity of nuclear TFEB–GFP fluorescence divided by the average of the cytosolic intensity of TFEB–GFP fluorescence. *P* values were calculated on the basis of mean values from independent fields.

RNA extraction, reverse transcription and quantitative PCR

RNA samples from cells were obtained using the RNeasy kit (Qiagen) and RNA samples from mouse kidneys were extracted using RNeasy plus Mini kit (Qiagen) according to the manufacturer's instructions. cDNA was synthesized using QuantiTect Reverse Transcription kit (Qiagen). Real-time quantitative RT–PCR on cDNAs was carried out with the LightCycler 480 SYBR Green I mix (Roche) using the Light Cycler 480 II detection system (Roche) with the following conditions: 95 °C, 5 min; (95 °C, 10 s; 60 °C, 10 s; 72 °C, 15 s) × 40. Fold change values were calculated using the $\Delta\Delta C_t$ method. In brief, internal controls (*HPRT1* or *B2M* for cell samples and cyclophilin (also known as *Ppia*) or *S16* (also known as *Rps16*) for mouse samples) were used as 'normalizer' genes to calculate the ΔC_t value. Next, the $\Delta\Delta C_t$ value was calculated between the 'control' group and the 'experimental' group. Finally, the fold change was calculated using $2(-\Delta\Delta C_t)$. Biological replicates were grouped in the calculation of the fold-change values.

Mouse models

All mice used were maintained in a C57BL/6 strain background.

The mouse line for conditional deletion of *Tfeb* (*Tfeb*$^{flox/flox}$) was previously described[19]. The mouse line for conditional deletion of *Flcn* (*Flcn*$^{flox/flox}$) and *Cdh16-cre* (*Ksp-cre*) were previously described[31,48] and acquired from Jackson Laboratories.

Survival curves were calculated for a period of 30 days (lethality time-frame for mice with kidney-specific *Flcn* knockout) on 30 *Flcn*$^{flox/flox}$*;Ksp-cre* mice and 29 *Flcn*$^{flox/flox}$*;Tfeb*$^{flox/flox}$*;Ksp-cre* mice grown in the same animal facility, all in same background (C57BL/6). Values were plotted by the product-limit method of Kaplan and Meier; statistical analyses were carried out applying the log–rank test.

To analyse serum blood urea nitrogen, blood was collected from mice at p2 from submandibular plexus, and from mice at p7, p14 and p21 from retro orbital plexus. Serum blood urea nitrogen content was measured by an ammonia colorimetric assay (BioVision; cat. no. K370-100) according to the manufacturer's instructions.

Histopathological analysis was conducted on formalin-fixed, paraffin-embedded kidney sections (3 µm) stained with H & E and images captured by using ImageScope (Leica-Biosystems Nussloch).

For immunohistochemical analysis of LAMP1, formalin-fixed, paraffin-embedded kidney sections (6 µm) were analysed by using the Vectastain ABC kit (Vector Labs) following the manufacturer's instructions. Signal was developed using 0.05% 3,3-diaminobenzidine tetrahydrochloride in 0.02% H_2O_2.

For staining of pS6 and of TFEB on kidney sections, OCT-embedded sections were cut at 7 µm, blocked and permeabilized in 3% (w/v) BSA, 5% goat serum in PBS + 0.3% Triton X-100 for 3 h and then were incubated with the primary antibody overnight. Finally sections were washed three times with 3% BSA in PBS + 0.3% Triton X-100 and then incubated for 1 h with secondary antibodies Alexa-Fluor-conjugated. Sections were mounted in VECTASHIELD mounting medium with DAPI and analysed using LSM 800 (Carl Zeiss).

To minimize variability, mice belonging to the same litter were grouped based on their genotype. All procedures on mice were approved by Italian Ministry of Health with the authorization code 240/2019. Mice were housed at the TIGEM animal house.

Statistical analysis

One-way analysis of variance (ANOVA) and Tukey's post hoc tests were performed when comparing more than two groups relative to a single factor.

Tukey multiple pairwise-comparisons for relative ratio of kidney to body weight were: at p14, *Flcn* knockout versus control *Flcn* $P = 4.9 \times 10^{-7}$, *Flcn* knockout versus control *Flcn Tfeb* $P = 3.04 \times 10^{-6}$, *Flcn* knockout versus *Flcn Tfeb* DKO $P = 3.6 \times 10^{-6}$, *Flcn Tfeb* DKO versus control *Flcn Tfeb* $P = 0.99$; at p21, *Flcn* knockout versus control *Flcn* $P = 1.08 \times 10^{-13}$, *Flcn* KO versus control *Flcn Tfeb* $P = 1.09 \times 10^{-13}$, *Flcn* knockout versus *Flcn Tfeb* DKO $P = 1.8 \times 10^{-12}$, *Flcn Tfeb* DKO versus control *Flcn Tfeb* $P = 0.99$.

Tukey multiple pairwise-comparisons for blood urea nitrogen were: at p7, *Flcn* knockout versus control *Flcn* $P = 1.2 \times 10^{-5}$, *Flcn* knockout versus control *Flcn Tfeb* $P = 6.5 \times 10^{-5}$, *Flcn* knockout versus *Flcn Tfeb* DKO $P = 6.5 \times 10^{-5}$, *Flcn Tfeb* DKO versus control *Flcn Tfeb* $P = 0.99$; at p14, *Flcn* knockout versus control *Flcn* $P = 1.1 \times 10^{-8}$, *Flcn* knockout versus control *Flcn Tfeb* $P = 5.4 \times 10^{-9}$, *Flcn* knockout versus *Flcn Tfeb* DKO $P = 9.8 \times 10^{-9}$, *Flcn Tfeb* DKO versus control *Flcn Tfeb* $P = 3.7 \times 10^{-2}$; at p21, *Flcn* knockout versus control *Flcn* $P = 1.3 \times 10^{-3}$, *Flcn* knockout versus control *Flcn Tfeb* $P = 1.4 \times 10^{-3}$, *Flcn* knockout versus *Flcn Tfeb*-DKO $P = 1.7 \times 10^{-3}$, *Flcn Tfeb* DKO versus control *Flcn Tfeb* $P = 0.99$.

Two-way ANOVA and Sidak's or Dunnett's post hoc tests were performed when comparing differences between groups that have been split on two factors. log–rank test was used for the survival analysis. $P < 0.05$ was considered significant.

Reporting summary

Further information on research design is available in the Nature Research Reporting Summary linked to this paper.

Data availability

Full scans for all western blots as well as raw data for all the graphs are provided with this manuscript. No datasets were generated or analysed during the current study. All other data are available from the corresponding author on reasonable request. Source data are provided with this paper.

45. Kawakami, K. *Tol2*: a versatile gene transfer vector in vertebrates. *Genome Biol.* **8**, S7 (2007).
46. de Araujo, M. E. G. et al. Crystal structure of the human lysosomal mTORC1 scaffold complex and its impact on signaling. *Science* **358**, 377–381 (2017).
47. Napolitano, G. et al. Impairment of chaperone-mediated autophagy leads to selective lysosomal degradation defects in the lysosomal storage disease cystinosis. *EMBO Mol. Med.* **7**, 158–174 (2015).
48. Shao, X., Johnson, J. E., Richardson, J. A., Hiesberger, T. & Igarashi, P. A minimal Ksp-cadherin promoter linked to a green fluorescent protein reporter gene exhibits tissue-specific expression in the developing kidney and genitourinary tract. *J. Am. Soc. Nephrol.* **13**, 1824–1836 (2002).

Acknowledgements We thank M. A. De Matteis, G. Diez-Roux, L. Murphy and C. Settembre for the critical reading of the manuscript; A. Iuliano for statistical analyisis; C. Soldati for software analysis of TFEB subcellular distribution; L. D'Orsi and N. Zampelli for technical help; and M. Mea for help in drawing the model figure. This work was supported by grants from the Italian Telethon Foundation 'TGM16CB6' (A.B.); MIUR 'PRIN 2017E5L5P3' (A.B) and 'PRIN 2017YF9FBS' (G.N.); European Research Council H2020 AdG 'LYSOSOMICS 694282' (A.B.); European Union's Horizon 2020 MSCA 'REBuILD 661271' (G.N.); US National Institutes of Health 'R01-NS078072' (A.B.); Huffington Foundation (A.B.); European Regional Development Fund - POR Campania FESR 2014/2020 (A.B); Associazione Italiana per la Ricerca sul Cancro A.I.R.C. 'IG-22103' and '5x1000-21051' (A.B.), 'MFAG-23538' (G.N.) and 'IG-18988' (P.P.D.F.); University of Naples 'Federico II' 'STAR L1 2018' (G.N.); MCO 10000 (P.P.D.F.); and Italian Ministry of Health 'RF-2016-02361540' (P.P.D.F.).

Author contributions G.N., C.D.M. and A.B. conceived the study. G.N., C.D.M. and A.E. designed the experiments. G.N. and M.M. performed the majority of co-immunoprecipitation and the in vitro experiments involving RagC. A.E. performed experiments involving FBS, RHEB and TSC2, TFEB chimaera and Lys- and Mit-RAPTOR. C.D.M. and A.Z. performed the experiments on FLCN-knockout HeLa cells, and generated and characterized the mouse lines described in the study. D.S. was involved in the characterization of mouse lines and analysis of RagA-knockout cells. C.V. was involved in some experiments on FLCN-knockout cells. E.N. helped with mouse handling. V.B. and A.V. performed some of the experiments involving Lys–RAPTOR. M.C. was involved in virus and cell line preparation. J.M. generated CRISPR–Cas9 gene-edited cell lines and performed some microscopy experiments. A.C. was involved in some of the experiments related to RHEB depletion. M.E.G.d.A., T.S. and L.A.H. performed and analysed biochemistry experiments. S.P., G.B. and P.P.D.F. performed and analysed histology experiments. G.N., C.D.M. and A.B. wrote the manuscript. A.B. supervised the study.

Competing interests A.B. is cofounder of CASMA Therapeutics, Inc.

Additional information

Supplementary information is available for this paper at https://doi.org/10.1038/s41586-020-2444-0.

Correspondence and requests for materials should be addressed to A.B.

Peer review information *Nature* thanks Kun-Liang Guan and the other, anonymous, reviewer(s) for their contribution to the peer review of this work. Peer reviewer reports are available.

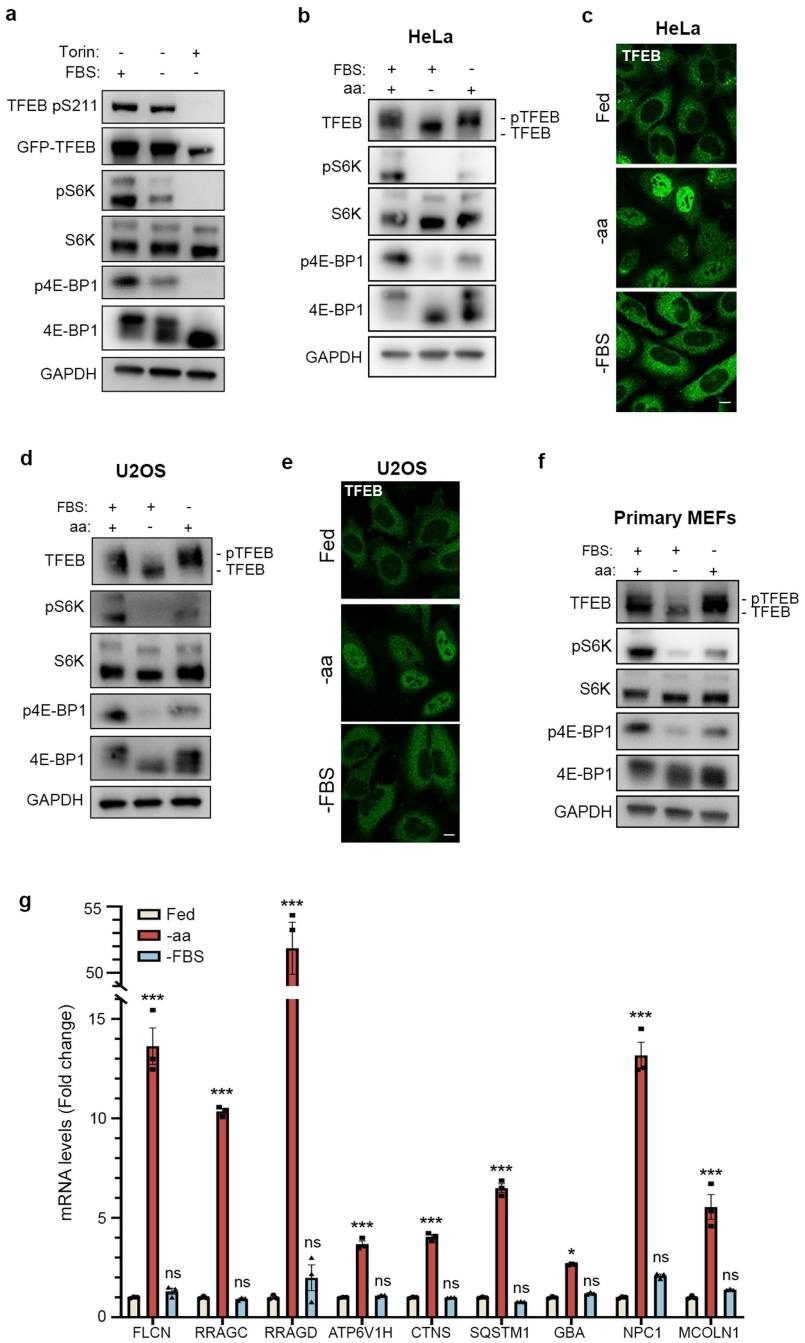

Extended Data Fig. 1 | TFEB phosphorylation is insensitive to serum starvation. a, HeLa cells stably expressing GFP–TFEB were starved of serum (FBS) for 2 h in the presence or absence of 250 nM torin and analysed by immunoblotting with the indicated antibodies (replicated twice). **b**–**f**, HeLa (**b**, **c**), U2OS (**d**, **e**) or primary MEFs (**f**) were starved of amino acids or serum for 2 h and then analysed by immunoblotting for the indicated proteins (**b**, **d**, **f**) or by immunofluorescence to assess TFEB subcellular localization (**c**, **e**) (replicated twice). Scale bars, 10 µm. **g**, HeLa cells stably expressing GFP–TFEB were either starved of amino acids (−aa) or serum (−FBS) for 8 h and subjected to qRT–PCR (replicated twice). Relative mRNA levels of the indicated genes were normalized to levels of *HPRT1* and expressed as fold change relative to control (fed) samples. Results are mean ± s.e.m.; $n = 3$; $^{*}P < 0.05$ (*GBA*, −aa $P = 0.0322$); $^{***}P < 0.001$ (*FLCN*, −aa $P < 0.0001$; *RRAGC*, −aa $P < 0.0001$; *RRAGD*, −aa $P < 0.0001$; *ATP6V1H*, −aa $P = 0.0004$; *CTNS*, −aa $P < 0.0001$; *SQSTM1*, −aa $P < 0.0001$; *NPC1*, −aa $P < 0.0001$; *MCOLN1*, −aa $P < 0.0001$); NS, non-significant (*FLCN*, −FBS $P = 0.8619$; *RRAGC*, −FBS $P = 0.99$; *RRAGD*, −FBS $P = 0.2558$; *ATP6V1H*, −FBS $P = 0.9890$; *CTNS*, −FBS $P > 0.9999$; *SQSTM1*, −FBS $P = 0.9270$; *GBA*, −FBS $P = 0.9359$; *NPC1*, −FBS $P = 0.1933$; *MCOLN1*, −FBS $P = 0.7916$). Dunnett's multiple comparisons test.

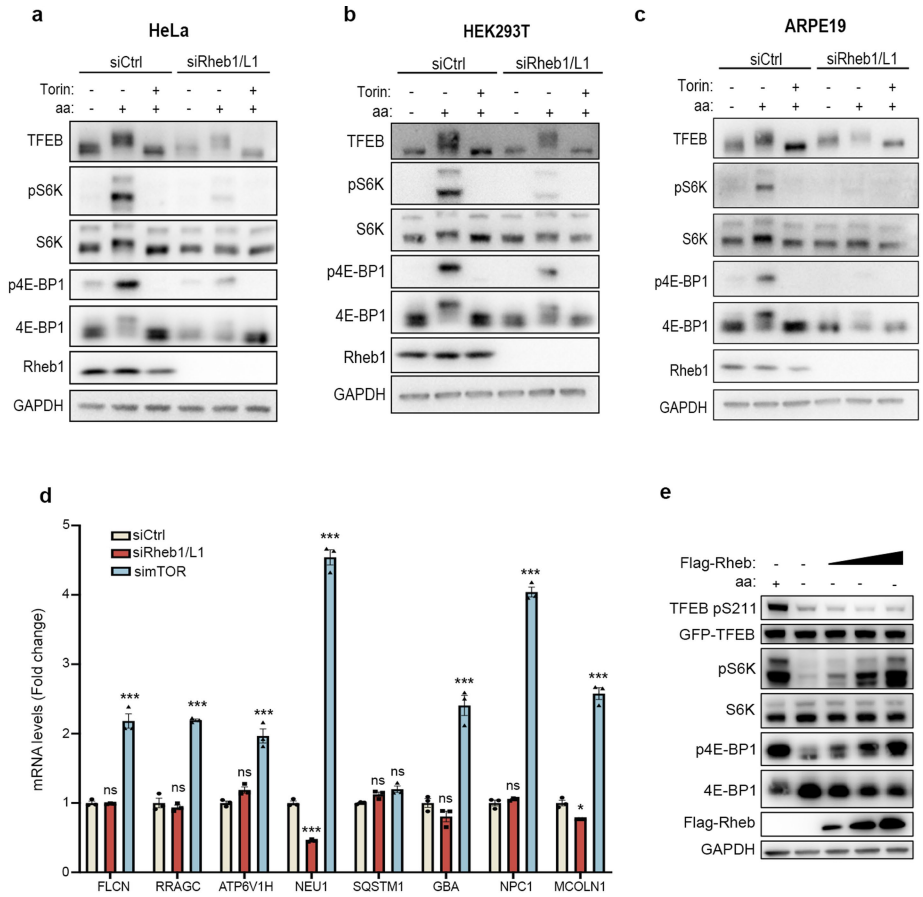

Extended Data Fig. 2 | TFEB phosphorylation is insensitive to the RHEB–TSC axis. a–**c**, HeLa (**a**), HEK293T (**b**) or ARPE19 (**c**) cells were transfected with either siRNA targeting both *RHEB* and *RHEBL1* or with scramble siRNA. Seventy-two hours after transfection cells were either starved of amino acids for 60 min or starved and restimulated with amino acids for 30 min, in the presence or absence of 250 nM torin, and analysed by immunoblotting with the indicated antibodies (replicated twice). **d**, HeLa cells stably expressing GFP–TFEB were transfected with siRNA targeting either *RHEB* and *RHEBL1* (siRHEB/L1), *MTOR* (simTOR), or control siRNA (siCtrl) for 72 h, and subjected to qRT–PCR (replicated three times). Relative mRNA levels of the indicated genes were normalized to levels of *HPRT1* and expressed as fold change relative to control (siCtrl) samples. Results are mean ± s.e.m.; $n = 3$; $^{*}P < 0.05$ (*MCOLN1*, siRHEB $P = 0.0212$); $^{***}P < 0.001$ (*FLCN*, siMTOR $P < 0.0001$; *RRAGC*, siMTOR $P < 0.0001$; *ATP6V1H*, siMTOR $P < 0.0001$; *NEU1*, siRHEB $P < 0.0001$; *NEU1*, siMTOR $P < 0.0001$; *GBA*, siMTOR $P < 0.0001$; *NPC1*, siMTOR $P < 0.0001$; *MCOLN1*, siMTOR $P < 0.0001$); ns, non-significant (*FLCN*, siRHEB $P = 0.9908$; *RRAGC*, siRHEB $P = 0.6937$; *ATP6V1H*, siRHEB $P = 0.0714$; *SQSTM1*, siRHEB $P = 0.2846$; *SQSTM1*, siMTOR $P = 0.0528$; *GBA*, siRHEB $P = 0.0597$; *NPC1*, siRHEB $P = 0.7753$). Dunnett's multiple comparisons test. **e**, HEK293A cells stably expressing GFP–TFEB, transfected with either empty vector or with increasing amounts of Flag–RHEB, were either left untreated or starved of amino acids for 60 min and analysed by immunoblotting (replicated three times).

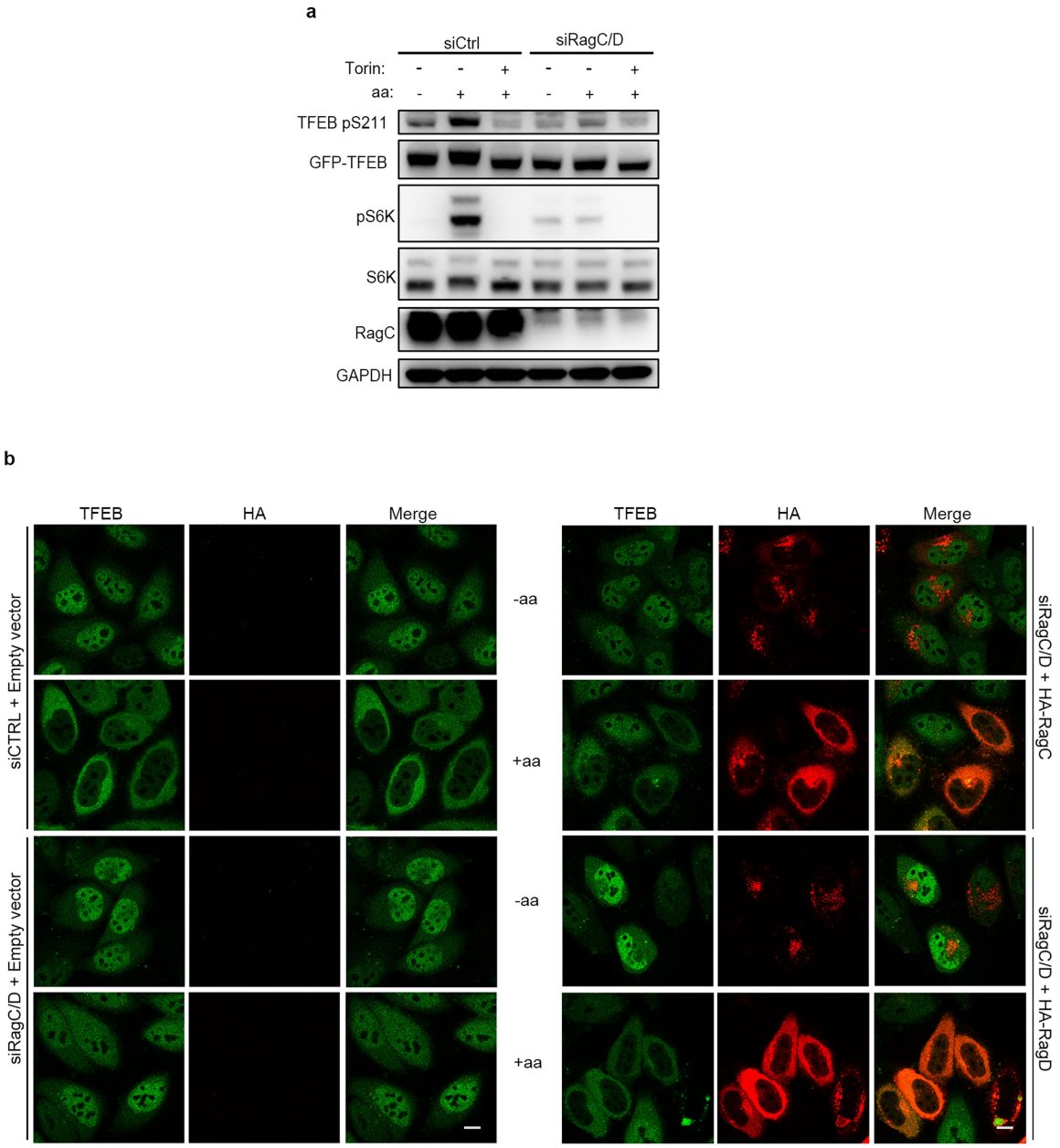

Extended Data Fig. 3 | Rag GTPases are required for TFEB phosphorylation. **a**, HeLa cells stably expressing GFP–TFEB were transfected with siRNAs targeting both *RRAGC* and *RRAGD* or with a control siRNA (siCtrl). Seventy-two hours after transfection, cells were either starved of amino acids for 60 min or starved and restimulated with amino acids for 30 min in the presence or absence of torin and analysed by immunoblotting using the indicated antibodies (replicated three times). **b**, Immunofluorescence analysis of TFEB localization in HeLa cells stably expressing GFP–TFEB and transfected with *RRAGC*- and *RRAGD*-targeting siRNA or with control siRNA (siCtrl) and after 48 h with empty vector (left), HA–RagC or HA–RagD (right). Cells were either starved for amino acids for 60 min (−aa) or starved and then restimulated with amino acids for 30 min (+aa) (replicated three times). Scale bar, 10 µm.

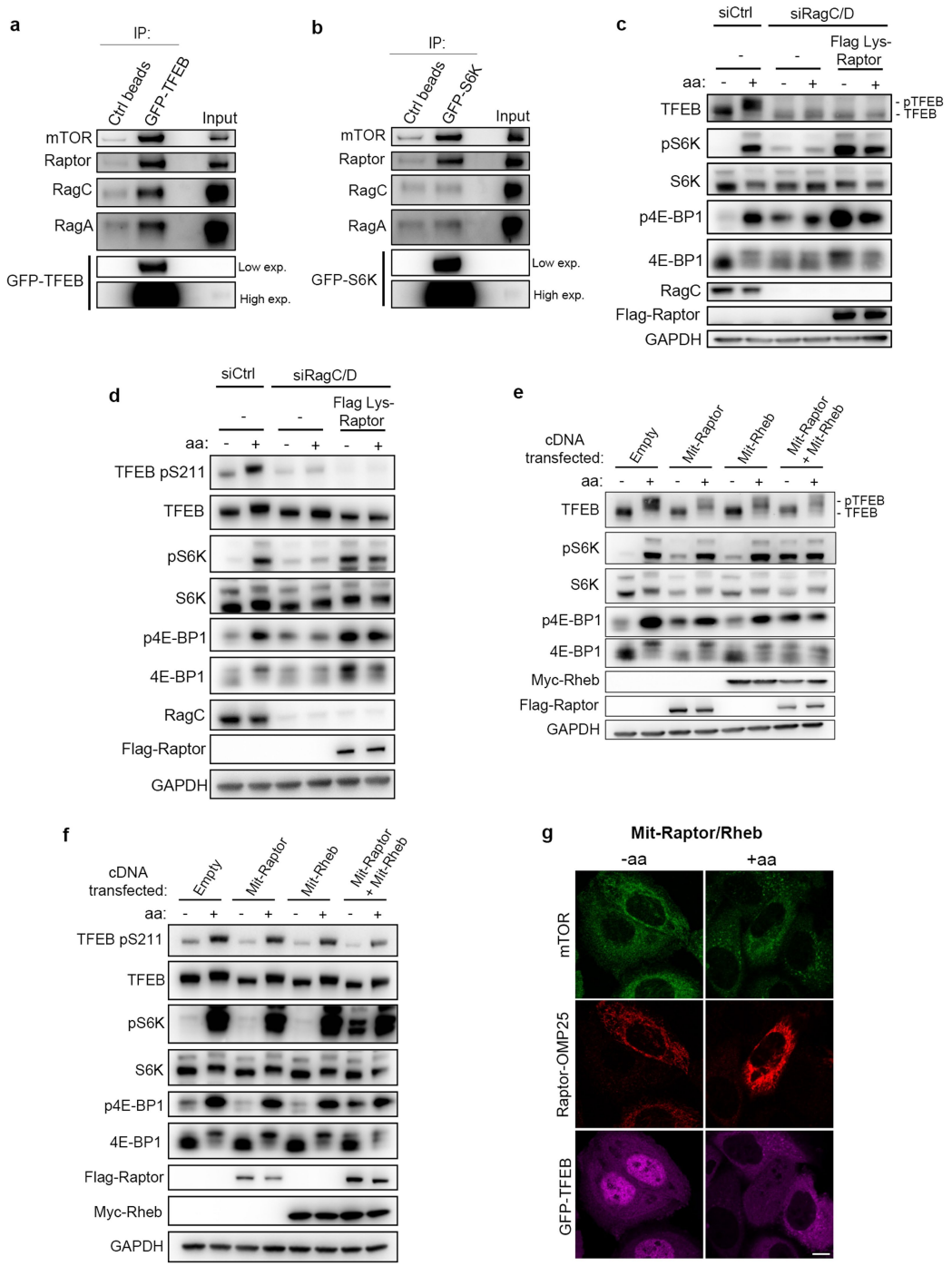

Extended Data Fig. 4 | Rag GTPases are required for TFEB phosphorylation regardless of mTORC1 activation status. a, **b**, GFP immunoprecipitates were prepared from HEK293A cells stably expressing GFP–TFEB (**a**) or GFP–S6K (**b**) and analysed by immunoblotting for the indicated proteins (replicated three times). **c**, **d**, HEK293T cells (**c**) or HeLa cells stably expressing GFP–TFEB (**d**) were transduced with lentiviruses expressing Lys–RAPTOR or with control lentiviruses and transfected with siRNA targeting both *RRAGC* and *RRAGD* (siRagC/D) or with scramble siRNA (siCtrl). Seventy-two hours after transfection, cells were either starved of amino acids for 60 min or starved and restimulated with amino acids for 30 min and analysed by immunoblotting using the indicated antibodies (replicated three times). **e**, **f**, HEK293T cells (**e**) or HeLa cells stably expressing GFP–TFEB (**f**) transiently expressing the indicated combinations of mitochondria-targeted RAPTOR (Mit-Raptor: Flag–RAPTOR–OMP25) and RHEB (Mit-Rheb: Myc–RHEB–OMP25) were starved of amino acids for 60 min or starved and re-stimulated with amino acids for 30 min and analysed by immunoblotting using the indicated antibodies (replicated three times). **g**, HeLa cells stably expressing GFP–TFEB were transfected and treated as in **f** and analysed by immunofluorescence for the indicated proteins. GFP–TFEB was pseudocoloured to magenta to allow better visualization of mTOR and RAPTOR–OMP25 staining (replicated three times). Scale bar, 10 μm.

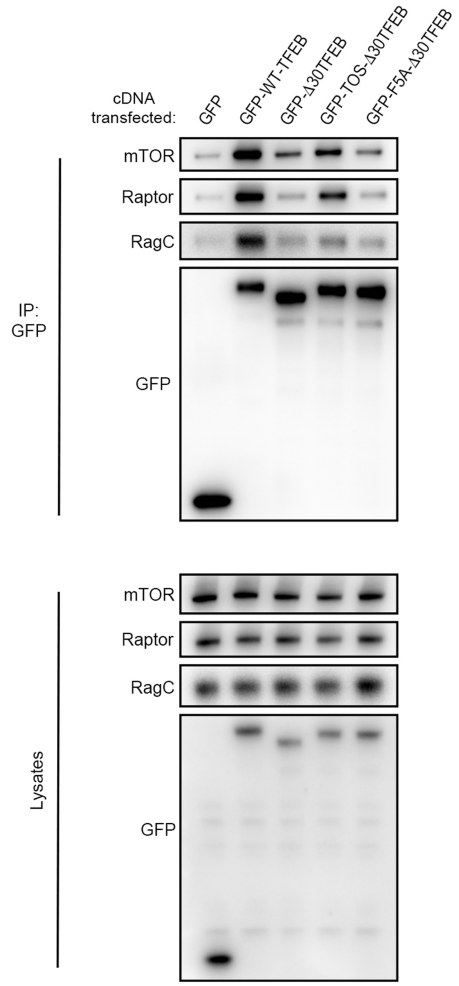

Extended Data Fig. 5 | The mTORC1 substrate-recruitment mechanism of TFEB is determined by its N-terminal region. HeLa cells were transiently transfected with plasmids expressing either GFP alone or GFP-tagged versions of the following proteins: TFEB (GFP–WT–TFEB), a TFEB deletion mutant that lacks the first 30 amino acids (GFP–Δ30TFEB), a chimeric protein in which the first 30 amino acids of S6K (containing the TOS motif) were fused to the D30TFEB mutant (GFP-TOS-Δ30TFEB), or the TOS-D30TFEB chimeric protein in which a key phenylalanine residue (F5) of the TOS motif was mutagenized to alanine (GFP-F5A-Δ30TFEB). Twenty-four hours after transfection cell lysates were incubated with GFP beads and subjected to immunoblotting using the indicated antibodies (replicated three times).

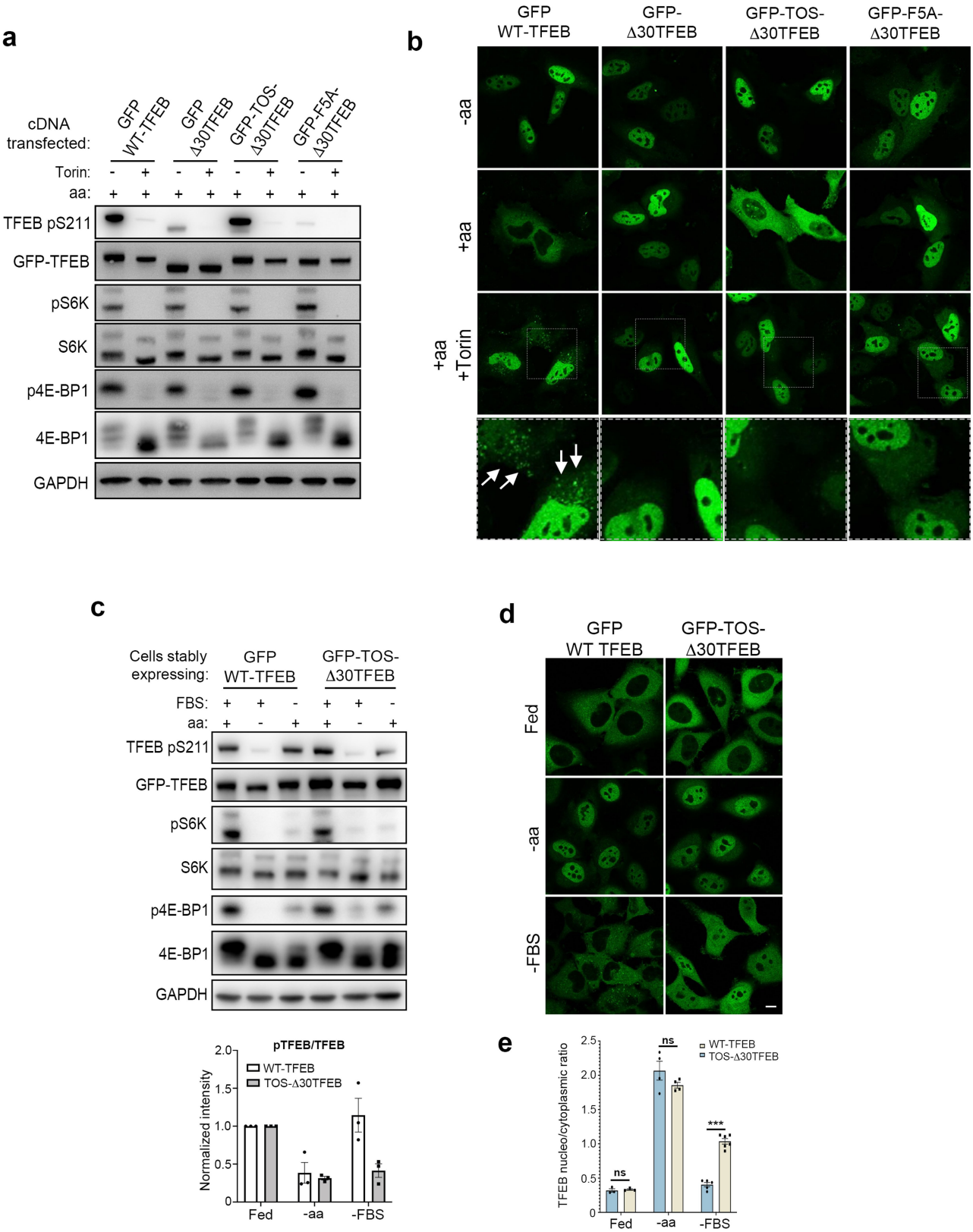

Extended Data Fig. 6 | See next page for caption.

Extended Data Fig. 6 | Addition of a TOS motif to a Rag-binding-deficient TFEB mutant rescues its phosphorylation and subcellular localization. **a**, HeLa cells transiently expressing the cDNAs described in Extended Data Fig. 5 were starved of amino acids for 60 min and restimulated with amino acids for 30 min, in the presence or absence of 250 nM torin, and analysed by immunoblotting using the indicated antibodies (replicated three times). **b**, Cells described in **a** were either starved of amino acids for 60 min or starved and restimulated with amino acids for 30 min, in the presence or absence of torin, and analysed for TFEB subcellular localization by immunofluorescence (replicated twice). **c**, Representative immunoblotting and quantification (mean ± s.e.m.; $n = 3$) of HeLa cells stably expressing GFP–TFEB or GFP–TOS-D30TFEB. Cells were either kept fed, starved of amino acids (−aa) or serum (−FBS) for 2 h. **d**, Cells described and treated as in **c** were analysed by immunofluorescence to assess TFEB subcellular localization (replicated three times). Scale bar, 10 μm. **e**, Analysis of TFEB localization performed using a dedicated script (Columbus software; Perkin-Elmer) that calculates the ratio value resulting from the average intensity of nuclear TFEB–GFP fluorescence divided by the average of the cytosolic intensity of TFEB–GFP fluorescence. Results are mean ± s.e.m. *P* values were calculated on the basis of mean values from 3 or 4 independent fields (Sidak's multiple comparisons test). ***$P < 0.0001$; NS, non-significant (fed, $P = 0.9989$; −aa, $P = 0.0946$).

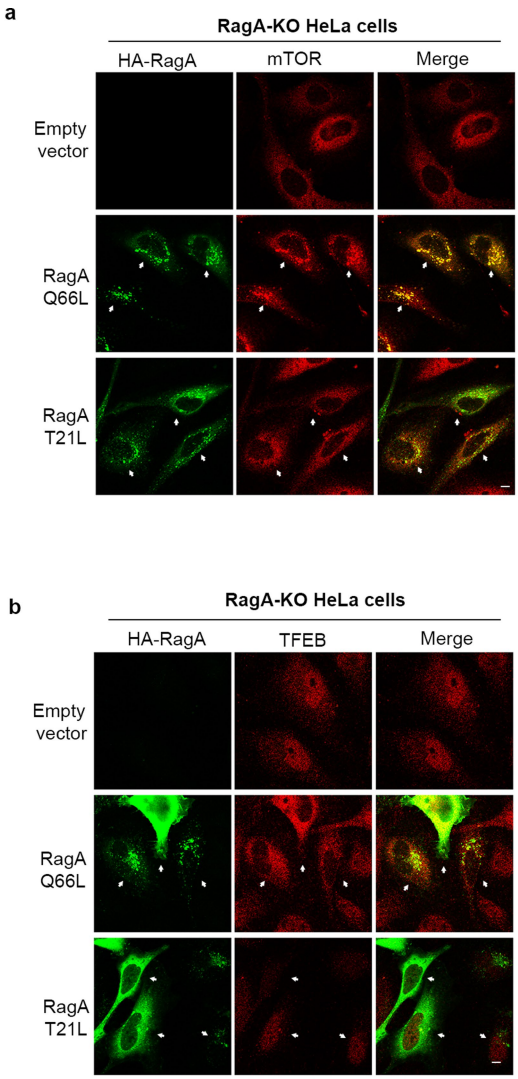

Extended Data Fig. 7 | Activation of RagA is essential for mTOR lysosomal recruitment and TFEB cytosolic localization. a, **b**, Representative immunofluorescence images of endogenous mTOR (**a**) and endogenous TFEB (**b**) upon transfection of a construct encoding active (RagA(Q66L)) or inactive (RagA(T21L)) HA-tagged RagA or an empty vector in RagA-knockout HeLa cells. Cells were deprived of amino acids for 50 min and then stimulated with amino acids for 15 min. Scale bars, 10 µm.

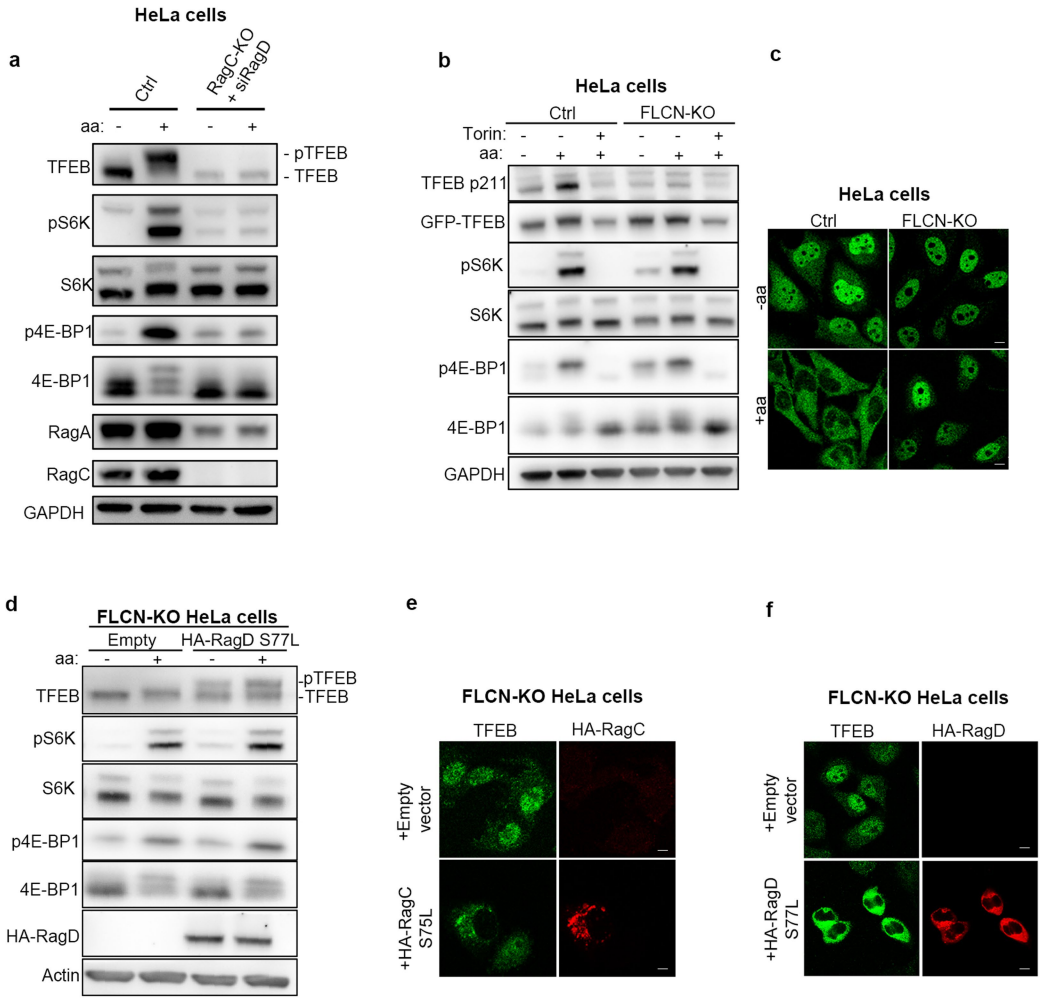

Extended Data Fig. 8 | TFEB phosphorylation and cytosolic retention requires active RagC/D. a, RagC-knockout HeLa cells were transfected with *RRAGD*-targeting siRNA (siRagD) for 72 h, then either starved of amino acids for 60 min or starved and restimulated with amino acids for 30 min and analysed by immunoblotting using the indicated antibodies (replicated three times). **b**, FLCN-knockout and control HeLa cells overexpressing the TFEB–GFP construct were either starved of amino acids for 60 min, or starved and restimulated with amino acids for 30 min in the presence or absence of 250 nM torin, and then analysed by immunoblotting with the indicated antibodies (replicated three times). **c**, Immunofluorescence analysis representative of triplicate experiments of TFEB in FLCN-knockout and control HeLa cells kept in amino acid deprived medium (−aa) or restimulated in amino-acid-containing medium (+aa). Scale bars, 10 µm. **d**, FLCN-knockout HeLa cells transfected with empty vector or with constitutively active RagD (RagD(S75L)) were either starved of amino acids for 60 min, or starved and restimulated with amino acids for 30 min, and analysed by immunoblotting with the indicated antibodies (replicated three times). **e**, **f**, FLCN-knockout Hela cells transfected with empty vector or constitutively active RagC (RagC(S75L)) (**d**) or constitutively active RagD (RagD(S77L)) (**e**) and kept in basal medium were immunostained with the indicated antibodies (replicated three times). Scale bars, 10 µm.

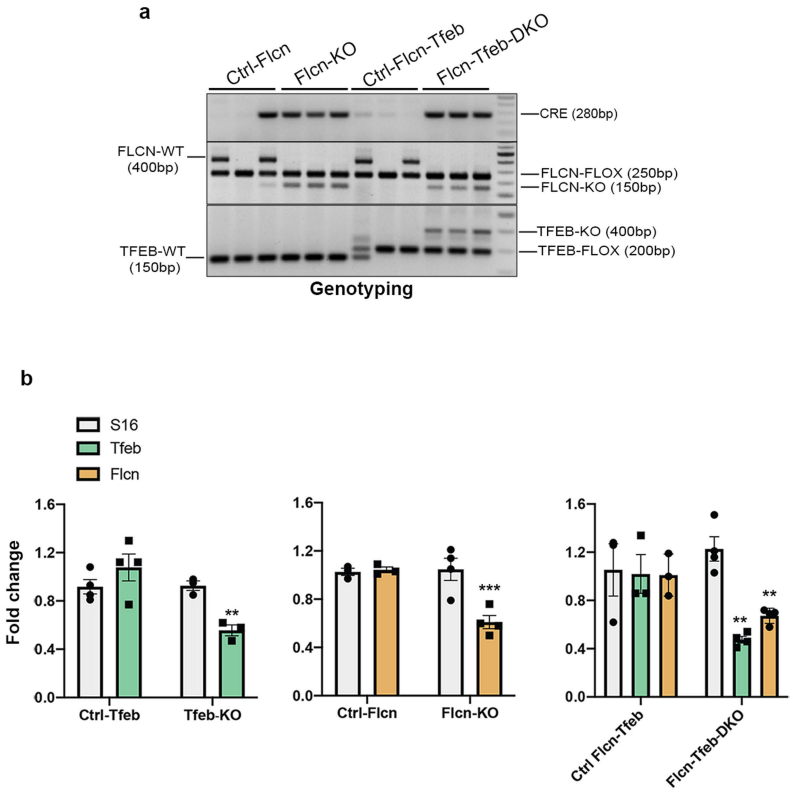

Extended Data Fig. 9 | Genomic and mRNA analysis of transgenic mouse lines. a, PCR analysis of genotypes from kidney samples of *Flcn*$^{flox/flox}$;*Ksp-cre*$^{+}$ (Flcn-KO) mice and *Flcn*$^{flox/flox}$;*Tfeb*$^{flox/flox}$;*Ksp-cre*$^{+}$ (Flcn-Tfeb-DKO) mice and corresponding controls (replicated three times). In detail, genotypes of Ctrl-Flcn mice were the following: *Flcn*$^{flox/+}$- *Flcn*$^{flox/flox}$ - *Flcn*$^{flox/+}$;*Ksp-cre*$^{+}$. Genotypes of Ctrl-Flcn-Tfeb mice were the following: *Flcn*$^{flox/+}$;*Tfeb*$^{flox/+}$-*Flcn*$^{flox/flox}$;*Tfeb*$^{flox/flox}$-*Flcn*$^{flox/+}$;*Tfeb*$^{flox/flox}$. **b**, mRNA levels of the indicated genes in *Tfeb*$^{flox/flox}$;*Ksp-cre*$^{+}$ (Tfeb-KO), *Flcn*$^{flox/flox}$;*Ksp-cre*$^{+}$ (Flcn-KO), *Flcn*$^{flox/flox}$;*Tfeb*$^{flox/flox}$;*Ksp-cre*$^{+}$(Flcn-Tfeb-DKO) and corresponding control mice at p2. Bars represent mean ± s.e.m. for each group and are expressed as fold change compared with control mice, normalized to cyclophilin gene expression. $^{**}P < 0.01$, $^{***}P < 0.001$, two-sided Student *t*-test. *S16* expression is shown as a control, unrelated gene ($n = 4$ Ctrl-Tfeb; $n = 3$ Tfeb-KO; $n = 3$ Ctrl-Flcn; $n = 4$ Flcn-KO; $n = 3$ Ctrl-Flcn-Tfeb; $n = 4$ Flcn-Tfeb-DKO).

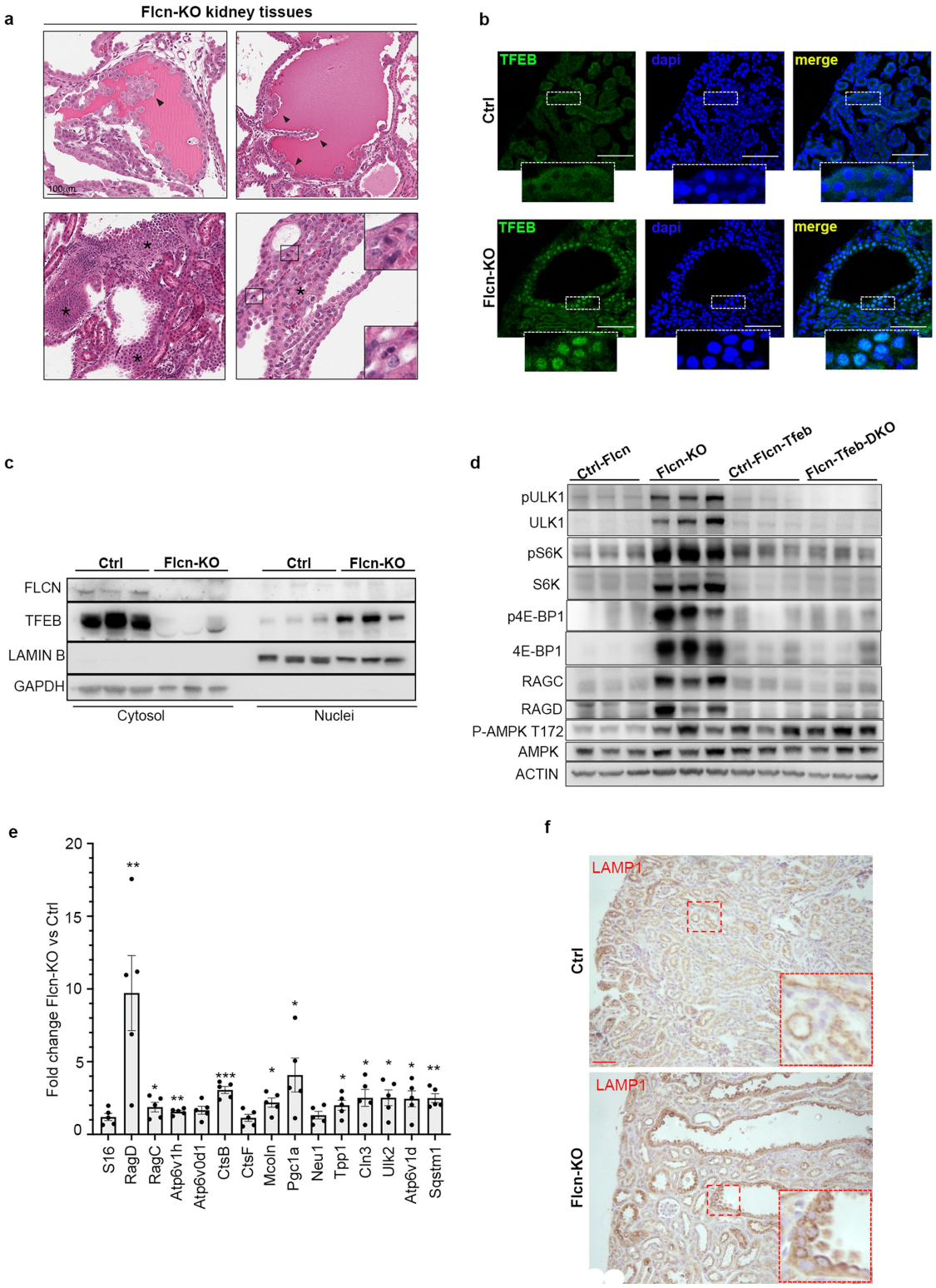

Extended Data Fig. 10 | See next page for caption.

Extended Data Fig. 10 | TFEB is constitutively nuclear and active in FLCN-knockout kidneys, and its depletion rescues mTORC1 hyperactivation. **a**, Representative images from three independent histopathological analyses of FLCN-knockout kidney tissues showing magnifications of areas with tubular papillary atypical hyperplasia (arrowheads, top), hyperplasia with considerable alterations of the tubular morphology (marked by asterisks in the bottom left panel) and atypical hyperplasia with multiple mitoses (represented in boxed areas and magnified in indents in bottom right panel). Scale bar, 100 µm. **b**, Representative immunofluorescence analysis of triplicate experiments of TFEB in kidney sections from mice of the indicated genotypes. Insets show higher magnification of the boxed area. Scale bars, 100 µm. **c**, Immunoblotting analysis of the indicated proteins in cytosolic and nuclear fractions of kidneys from *Flcn*$^{flox/flox}$ (Ctrl) and *Flcn*$^{flox/flox}$*;Ksp-cre*$^{+}$ (Flcn-KO) mice (replicated three times). **d**, Immunoblotting analysis of the indicated proteins in kidneys from *Flcn*$^{flox/flox}$*;Ksp-cre*$^{+}$ (Flcn-KO) mice and *Flcn*$^{flox/flox}$*;Tfeb*$^{flox/flox}$*; Ksp-cre*$^{+}$ (Flcn-Tfeb-DKO) mice and corresponding controls (replicated three times). **e**, mRNA levels of several TFEB target genes were analysed in kidney samples from FLCN-knockout mice relative to control mice. Bars represent mean ± s.e.m. for $n = 5$ mice for each group and are expressed as fold change compared with control mice, normalized to cyclophilin gene expression. $^{*}P < 0.05$, $^{**}P < 0.01$, $^{***}P < 0.001$, two-sided Student *t*-test. *S16* expression is shown as a control, unrelated gene. **f**, Immunohistochemical analysis of LAMP1 in kidney sections from FLCN-knockout mice and control mice (replicated three times). Insets show higher magnification of the boxed area. Scale bars, 50 µm. In **a**–**f**, analysis was performed on 21-day-old mice.

nature research

Corresponding author(s): Andrea Ballabio

Last updated by author(s): Apr 16, 2020

Reporting Summary

Nature Research wishes to improve the reproducibility of the work that we publish. This form provides structure for consistency and transparency in reporting. For further information on Nature Research policies, see Authors & Referees and the Editorial Policy Checklist.

Statistics

For all statistical analyses, confirm that the following items are present in the figure legend, table legend, main text, or Methods section.

n/a	Confirmed	
☐	☒	The exact sample size (*n*) for each experimental group/condition, given as a discrete number and unit of measurement
☐	☒	A statement on whether measurements were taken from distinct samples or whether the same sample was measured repeatedly
☐	☒	The statistical test(s) used AND whether they are one- or two-sided *Only common tests should be described solely by name; describe more complex techniques in the Methods section.*
☒	☐	A description of all covariates tested
☐	☒	A description of any assumptions or corrections, such as tests of normality and adjustment for multiple comparisons
☐	☒	A full description of the statistical parameters including central tendency (e.g. means) or other basic estimates (e.g. regression coefficient) AND variation (e.g. standard deviation) or associated estimates of uncertainty (e.g. confidence intervals)
☐	☒	For null hypothesis testing, the test statistic (e.g. *F*, *t*, *r*) with confidence intervals, effect sizes, degrees of freedom and *P* value noted *Give P values as exact values whenever suitable.*
☒	☐	For Bayesian analysis, information on the choice of priors and Markov chain Monte Carlo settings
☒	☐	For hierarchical and complex designs, identification of the appropriate level for tests and full reporting of outcomes
☒	☐	Estimates of effect sizes (e.g. Cohen's *d*, Pearson's *r*), indicating how they were calculated

Our web collection on statistics for biologists contains articles on many of the points above.

Software and code

Policy information about availability of computer code

Data collection	Zeiss Zen Blue 2.1 software
Data analysis	Graphpad Prism 8; Fiji 1.0; Microsoft Excel 2020; Columbus 2.6.0, Perkin Elmer;

For manuscripts utilizing custom algorithms or software that are central to the research but not yet described in published literature, software must be made available to editors/reviewers. We strongly encourage code deposition in a community repository (e.g. GitHub). See the Nature Research guidelines for submitting code & software for further information.

Data

Policy information about availability of data

All manuscripts must include a data availability statement. This statement should provide the following information, where applicable:

- Accession codes, unique identifiers, or web links for publicly available datasets
- A list of figures that have associated raw data
- A description of any restrictions on data availability

Full scans for all western blots are provided in Supplementary Fig. 1. Raw data for all the graphs are provided in Supplementary Fig. 2. No datasets were generated or analyzed during the current study. All other data are available from the corresponding author on reasonable request.

Field-specific reporting

Please select the one below that is the best fit for your research. If you are not sure, read the appropriate sections before making your selection.

☒ Life sciences ☐ Behavioural & social sciences ☐ Ecological, evolutionary & environmental sciences

Life sciences study design

All studies must disclose on these points even when the disclosure is negative.

Sample size	The sample size was chosen based on previous experience with respect to how many independent cohorts and number of mice or number of cells per treatment group are required to reliably detect biologically meaningful differences among groups.
Data exclusions	We did not apply any exclusion criteria
Replication	All experiments were carried out under standard and clearly defined conditions, and were replicated successfully by at least one researcher. All attempts at replication were successful.
Randomization	To minimize variability, mice belonging to the same litter were grouped based on their genotype
Blinding	Investigators were blinded for immunofluorescence analysis.

Reporting for specific materials, systems and methods

We require information from authors about some types of materials, experimental systems and methods used in many studies. Here, indicate whether each material, system or method listed is relevant to your study. If you are not sure if a list item applies to your research, read the appropriate section before selecting a response.

Materials & experimental systems

n/a	Involved in the study
☐	☒ Antibodies
☐	☒ Eukaryotic cell lines
☒	☐ Palaeontology
☐	☒ Animals and other organisms
☒	☐ Human research participants
☒	☐ Clinical data

Methods

n/a	Involved in the study
☒	☐ ChIP-seq
☒	☐ Flow cytometry
☒	☐ MRI-based neuroimaging

Antibodies

Antibodies used

Antibodies to RagC (Cat# 3360 - 1:1000 dilution), RagA (Cat# 4357 - 1:1000 dilution), RagD (# 4470 - 1:1000 dilution) mTOR (Cat# 2983 - 1:1000 (WB)/ 1:100 (IF) dilution) Phospho-p70 S6 Kinase (Thr389) (1A5) (Cat# 9206 - 1:1000 dilution), p70 S6 Kinase (Cat# 9202 - 1:1000 dilution), Rheb1 (Cat# 13879 - 1:1000 dilution), 4E-BP1 (Cat# 9644 - 1:1000 dilution), Phospho-4E-BP1 (Ser65) (Cat# 9456 - 1:1000 dilution), Raptor (24C12) (# 2280 - 1:1000 dilution), human TFEB (Cat# 4240 - 1:1000 (WB)/ 1:100 (IF) dilution), Tuberin/TSC2 (Cat# 4308 - 1:1000 dilution), FLCN (# 3697 - 1:1000 dilution), Phospho -ULK1 (# 6888 - 1:1000 dilution), pan-ULK1 (# 8054 - 1:1000 dilution), Phospho -AMPK (T172) (# 2535 - 1:1000 dilution), anti-AMPK (# 2532 - 1:1000 dilution), Phospho-S6 (# 5364 - 1:100 (IF) dilution) and Myc-Tag (# 2276 - 1:1000 dilution) were from Cell Signaling Technology; antibody to GFP (Cat# ab13970) was from Abcam; antibodies to GAPDH (6C5) (Cat# sc-32233 - 1:15000 dilution), LAMP-1 (H4A3) (Cat# sc-20011 - 1:500 (IF) dilution), LAMP-1 (1D4B) (Cat# sc-19992 - 1:200 IHC), Lamin B (Cat# sc-6216 - 1:1000 dilution) were from Santa Cruz; antibodies to FLAG M2 (Cat# F1804 - 1:1000 dilution) and Actin (#A2228 - 1:5000 dilution) were from Sigma Aldrich; antibody to HA.11 Epitope Tag (Cat# 901513 - 1:1000 dilution) was from Biolegend; antibody to TFEB (Cat# A303-673A - 1:1000 (WB)/ 1:200 (IF) dilution) and RagD (A304-301A - 1:1000 dilution) was from Bethyl laboratories; HRP-conjugated secondary antibodies to Mouse (Cat# 401215 - 1:5000 dilution) and Rabbit (Cat# 401315 - 1:5000 dilution) IgGs were form Calbiochem; Donkey anti-Rabbit IgG (H+L) Alexa Fluor 488 (Cat# A-21206 - 1:500 dilution), Alexa Fluor 568 (Cat# A-10042 - 1:500 dilution), Donkey anti-mouse IgG (H+L) Alexa Fluor 568 (Cat# A-10037 - 1:500 dilution), Alexa Fluor 647 (Cat# A-31571 - 1:500 dilution), Alexa Fluor 594 (Cat# A-21203 - 1:500 dilution), Donkey anti-goat IgG (H+L) Alexa Fluor 647 (Cat# A-21447 - 1:500 dilution) were from Thermo Fisher Scientific; antibodies to TFEB-pS211 (used at 1:1000 dilution) were custom generated in collaboration with Bethyl Laboratories.
Throughout the study, several lots of each antibody may have been used, and each lot behaved similarly for the experimental purposes.

Validation

Most of the antibodies used in the study were bought from commercial vendors and were validated by the manufacturers and/ or other studies. Some of the antibodies were further validated using KO/knocked-down cell lines. See individual antibody's web page (link shown below)on the manufacture's website for validation and relevant citations:
- RagC: https://www.cellsignal.com/products/primary-antibodies/ragc-antibody/3360
- RagA: https://www.cellsignal.com/products/primary-antibodies/raga-d8b5-rabbit-mab/4357
- RagD: https://www.cellsignal.com/products/primary-antibodies/ragd-antibody/4470
- mTOR: https://www.cellsignal.com/products/primary-antibodies/mtor-7c10-rabbit-mab/2983
- Phospho-p70 S6 Kinase (Thr389): https://www.cellsignal.com/products/primary-antibodies/phospho-p70-s6-kinase-thr389-1a5-mouse-mab/9206
- p70 S6 Kinase: https://www.cellsignal.com/products/primary-antibodies/p70-s6-kinase-antibody/9202

- Rheb1: https://www.cellsignal.com/products/primary-antibodies/rheb-e1g1r-rabbit-mab/13879
- 4E-BP1: https://www.cellsignal.com/products/primary-antibodies/4e-bp1-53h11-rabbit-mab/9644
- Phospho-4E-BP1 (Ser65): https://www.cellsignal.com/products/primary-antibodies/phospho-4e-bp1-ser65-174a9-rabbit-mab/9456
- Raptor (24C12): https://www.cellsignal.com/products/primary-antibodies/raptor-24c12-rabbit-mab/2280
- Human TFEB: https://www.cellsignal.com/products/primary-antibodies/tfeb-antibody/4240
- Tuberin/TSC2: https://www.cellsignal.com/products/primary-antibodies/tuberin-tsc2-d93f12-xp-rabbit-mab/4308
- FLCN: https://www.cellsignal.com/products/primary-antibodies/flcn-d14g9-rabbit-mab/3697
- Phospho -ULK1: https://www.cellsignal.com/products/primary-antibodies/phospho-ulk1-ser757-antibody/6888
- pan-ULK1: https://www.cellsignal.com/products/primary-antibodies/ulk1-d8h5-rabbit-mab/8054
- Phospho -AMPK (T172): https://www.cellsignal.com/products/primary-antibodies/phospho-ampka-thr172-40h9-rabbit-mab/2535
- anti-AMPK: https://www.cellsignal.com/products/primary-antibodies/ampka-antibody/2532
- Phospho-S6: https://www.cellsignal.com/products/primary-antibodies/phospho-s6-ribosomal-protein-ser240-244-d68f8-xp-rabbit-mab/5364
- Myc-Tag: https://www.cellsignal.com/products/primary-antibodies/myc-tag-9b11-mouse-mab/2276
- GFP: https://www.abcam.com/gfp-antibody-ab13970.html
- GAPDH (6C5): https://www.scbt.com/p/gapdh-antibody-6c5
- LAMP-1 (H4A3): https://www.scbt.com/p/lamp-1-antibody-h4a3
- LAMP-1 (1D4B): https://www.scbt.com/p/lamp-1-antibody-1d4b
- Lamin B: https://www.scbt.com/p/lamin-b-antibody-c-20
- FLAG M2: https://www.sigmaaldrich.com/catalog/product/sigma/f1804
- Actin: https://www.sigmaaldrich.com/catalog/product/sigma/a2228
- HA.11 Epitope Tag: https://www.biolegend.com/en-us/products/anti-ha-11-epitope-tag-antibody-11071
- TFEB: https://www.bethyl.com/product/A303-673A/TFEB+Antibody
- RagD: https://www.bethyl.com/product/A304-301A/RRAGD+Antibody
- TFEB-pS211 was custom generated at Bethyl and tested by using TFEB plasmids carrying a mutation on the phosphorylation site (TFEB S211A)

Eukaryotic cell lines

Policy information about cell lines

Cell line source(s)	HeLa, HEK293T, ARPE-19 and U2OS cells were purchased from ATCC. WT and RagA/B-KO HEK293A were a kind gift from Kun-Liang Guan (University of California, San Diego). FLCN-KO HeLa cells were kindly provided by Zoltan Pierre Arany (University of Pennsylvania, Philadelphia, PA). RagC-KO and RagA-KO cells were generated in this study.
Authentication	KO cells were authenticated by WB or RT-PCR. Commercial cell lines were purchased recently from ATCC and validated by morphological analysis
Mycoplasma contamination	Cells were routinely tested and validated for the absence of mycoplasma
Commonly misidentified lines (See ICLAC register)	No commonly misidentified lines were used.

Animals and other organisms

Policy information about studies involving animals; ARRIVE guidelines recommended for reporting animal research

Laboratory animals	All mice used were maintained in a C57BL/6 strain background. Both males and females were used for the study. Mice were sacrificed at post-natal (p) day p-2, p7, p14 and p21. Kidney-specific Flcn-KO mice were all dead before 30 days of life. Kidney-specific Flcn-Tfeb-KO mice were indistinguishable from litter-mate controls up to 11 months of observation.
Wild animals	The study did not involve wild animals.
Field-collected samples	The study did not involve field-collected samples.
Ethics oversight	All procedures on mice were approved by Italian Ministry of Health with the authorization code 240/2019.

Note that full information on the approval of the study protocol must also be provided in the manuscript.